AD-A173 291 THE EFFECT OF CUTOUTS ON STRENGTH OF GRP (GLASS REINFORCED PLASTIC) FOR N..(U) MASSACHUSETTS INST OF TECH CAMBRIDGE DEPT OF OCEAN ENGINEERIN.. K M ADAMS 1/1

UNCLASSIFIED JUN 86 N00228-85-G-3262 F/G 11/4 NL

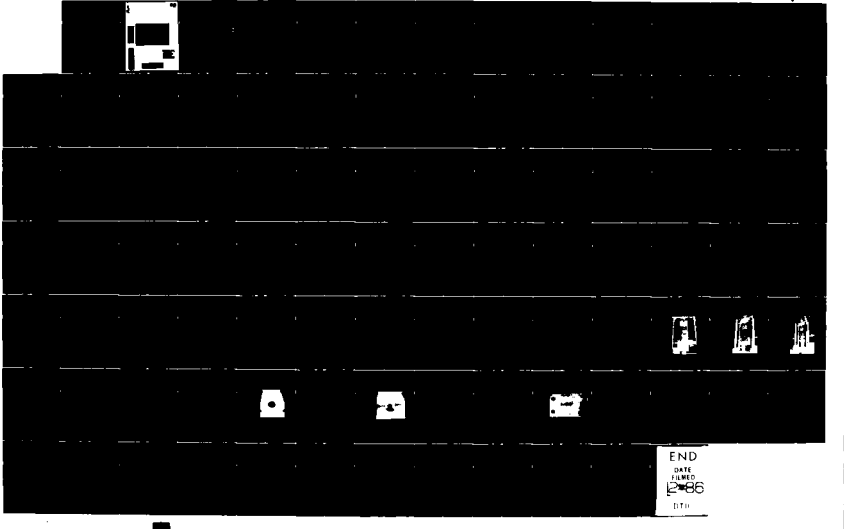

END
DATE FILMED
DTIC

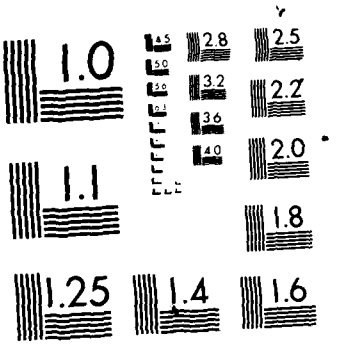

DEPARTMENT OF OCEAN ENGINEERING

MASSACHUSETTS INSTITUTE OF TECHNOLOGY

CAMBRIDGE, MASSACHUSETTS 02139

THE EFFECT OF CUTOUTS ON STRENGTH OF GRP FOR NAVAL SHIP HULLS

by

Kevin MacGregor Adams

Ocean Engineering - Course XIIIA
Materials Science and Engineering - Course III

June 1986

THE EFFECT OF CUTOUTS ON STRENGTH OF GRP FOR NAVAL SHIP HULLS

by

KEVIN MACGREGOR ADAMS
B.S. Cer.E., Rutgers University (1981)

Submitted to the Department of
Ocean Engineering
in Partial Fulfillment of the
Requirements of the Degrees of

MASTER OF SCIENCE IN
NAVAL ARCHITECTURE AND MARINE ENGINEERING
and
MASTER OF SCIENCE IN
MATERIALS SCIENCE AND ENGINEERING

at the

MASSACHUSETTS INSTITUTE OF TECHNOLOGY
June, 1986

Signature of Author _____
Department of Ocean Engineering, 9 May 1986

Certified by _____
Dr. John F. Mandell, Thesis Supervisor
Department of Materials Science and Engineering

Certified by _____
Professor Frederick J. McGarry, Thesis Supervisor
Department of Materials Science and Engineering

Certified by _____
Professor William D. Whiddon, Thesis Reader
Department of Ocean Engineering

Accepted by _____
Professor A. Douglas Charmichael, Chairman
Ocean Engineering Department Graduate Committee

Accepted by _____
Professor Bernhardt J. Wuensch, Chairman
Materials Science Department Graduate Committee

THE EFFECT OF CUTOUTS ON STRENGTH OF GRP FOR NAVAL SHIP HULLS

by

KEVIN MACGREGOR ADAMS

Submitted to the Department of Ocean Engineering
on 09 May 1986 in Partial Fulfillment of the
Requirements for the Degrees of

MASTER OF SCIENCE IN
NAVAL ARCHITECTURE AND MARINE ENGINEERING
and
MASTER OF SCIENCE IN
MATERIALS SCIENCE AND ENGINEERING

ABSTRACT

The effects of cutouts on the strength of glass reinforced plastic (GRP) for use in naval ship hulls have been studied. Experiments were conducted on an E-glass fiber/polyester resin laminate provided by the U.S. Navy Minesweeper Hunter (MSH) shipbuilder in 48 in. x 15 in. panels. Tensile tests were run on full-sized panels with circular cutouts of 3.75 to 7.50 inch diameter with and without edge notches; conventional tensile and fracture toughness tests were also run.

Three theoretical models were evaluated. First, the notch sensitivity was evaluated, and the material was found to be notch sensitve, so that models which include stress concentration effects are required. A simple stress concentration model appears valid, but can only provide an accurate prediction when the measured tensile strength is increased by a factor to represent the actual local strength at the cutout edge. Linear elastic fracture mechanics provides strength predictions reasonably close to the experimental results when cracks are present at the edge of the cutout.

In addition to the direct experimental results of the study, the effects of a seawater environment and cyclic fatigue loading are estimated based on earlier studies. The

overall effects on ship hull design safety factors are calculated. The required safety factors are excessively high unless cutouts are reinforced to eliminate the stress concentration effect. Detailed recommendations for further research and development needed to advance failure analysis in GRP hulls are provided.

Thesis Supervisors: Frederick J. McGarry and John F.Mandell
Title: Professor of Polymer Engineering and
Professor of Civil Engineering, and
Principal Research Associate

ADMINISTRATIVE INFORMATION

The funding necessary for this thesis has been provided by the United States Navy under contract N00167-86-N-2088. The work was sponsored by the David W. Taylor Naval Ship Research and Development Center (DTNSRDC) Structures Group, and was managed by Dr. M. O. Critchfield of Code 1730.2. This work provides resolution for a portion of the technology gap in fracture mechanics reported in Reference [1].

ACKNOWLEDGEMENTS

There are many people I wish to thank for their help in this endeavor. First and foremost is my thesis advisor, Professor Frederick J. McGarry. It was he who planted the seed that developed into an interest in composite materials. Dr. John F. Mandell, who provided technical guidance, prodding and counsel on an almost daily basis. To Professor William D. Whiddon, my thesis reader, for directing my efforts and providing a great deal of moral support throughout.

To my colleagues in the Materials Science Department, Walt McDonough and Andreas Echtermeyer, for their help in conducting strain measurements. To Professor Paul Legace and Doug Cairns of the Technology Laboratory for Advanced Composites (TELAC) for their help in designing the grip system used in the experiments. A special thanks to Paul Doyle, Bob Pasternak and Alice Fuller of the U. S. Army Materials Technology Laboratory in Watertown for their help in conducting the experiments.

My deepest gratitude goes to LT Chris Cable, USN, who is currently serving as the MSH Project Manager's Representative to Bell Aerospace in New Orleans. Chris provided the framework for the thesis and the unending support that made this thesis a reality.

Finally, I would like to thank my wife, Claire, whose patience, sacrifice and encouragement were instrumental in the successful completion of this thesis. And my children, Jennifer, Brian and Kristen who provided many hours of joy and love during this demanding period.

TABLE OF CONTENTS

LIST OF TABLES

LIST OF FIGURES

LIST OF APPENDICES

CHAPTER 1

INTRODUCTION

This thesis investigates the effect of flaws on Glass Reinforced Plastic (GRP) strength. Experiments have been designed to measure the effect which holes with edge cracks have on laminate strength in a GRP plate of E-glass fiber (woven roving and chopped strand mat) in a polyester resin, which is a typical naval ship hull material. This material is of particular interest because of the impending construction of the U. S. Navy's 434 ton Minesweeper Hunter (MSH), which is under contract to Bell Aerospace Corporation. This represents the U. S. Navy's first attempt to use GRP in a large ship hull, thus the program is under scrutiny both from within and outside of the Department of the Navy.

This thesis presents experimental data which, when correlated with the appropriate theoretical failure models, may provide a better understanding of the relationship between flaws and strength in a GRP naval ship hull. It is hoped that any new understanding will permit more reasonable factors of safety in the design of GRP ships which should allow GRP to be considered for the new generation of weight-limited, high performance ships required by a modern U. S. Navy [2].

CHAPTER 2

BACKGROUND

Overview

The use of glass reinforced plastics in the ocean engineering industry began in World War II. At that time GRP represented a new material with the strength, stability, low weight, environmental resistance and ease of fabrication needed for high-volume production of large marine parts such as boat hulls [3]. Only the high cost of raw materials and the slow, expensive processing methods of this period prevented its widespread use as a hull material. As shown in Table 1, the advantages of GRP now outweigh the disadvantages in naval ship hull and structural uses [4]. The significance of the advantages are clear when we view the demand for GRP during the last ten years. Table 2 presents data for GRP end use and shows that the growing total demand has been paralleled in the marine industry [5]. At the present time GRP materials are being used in the construction of boats, buoys, control surfaces, deckhouses, fairings, masts, propeller shrouds, protective coatings, radomes, sonar domes, pipes and other applications.

Hull Structures

Of particular interest is the use of GRP in naval ship hulls. The U. S. Navy pioneered fiberglass boat construction with the production of a 28 foot hull in 1947 and was influential in the use of hand lay-up procedures using woven roving and fire retardant polyester resins for boat hulls [6]. In 1951 a development contract was awarded for the construction of a minesweeping boat (MSB) with a structural sandwich core hull. The 57 foot boat was launched in 1956 and served satisfactorily for over 10 years [7,8]. By 1973 the Royal Navy had launched what was then the world's largest fiberglass ship, H.M.S. WILTON, a 153 foot, 450 ton minesweeper which used a mono-skin for its hull [9]. The success achieved in the H.M.S. WILTON prompted most of the world's navies to adopt the use of GRP in mine warfare ship hulls. Table 3 is a summary of existing mine warfare ships [10]. However, these ships have not been without their problems, the most predominant may be the presence of defects and their effect on the structural integrity of the ship hull [11].

Hull Defects

Thomas and Cable [11] have investigated the important defects in GRP naval ship hulls and classify the driving material defects as Type A or Type B. Type A are gross defects while Type B are more subtle and include voids, delaminations, reinforcement discontinuities, holes and notches. The Type B defects are considered to be more common and to have the greatest potential for property degradation [12].

With the use of modern Quality Assurance procedures all of the Type A and many of the Type B defects can be detected, evaluated, and corrected during production. However, when the remaining defects are placed in the context of a naval ship hull, the most deleterious effect was predicted to be [11] due to unreinforced hull cutouts (holes) and the resulting stress concentrations. This conclusion is based upon the tremendous number of relatively large hull penetrations that must exist in a ship for access, piping and wiring runs. The magnitude of the problem increases because these openings will have to be cut out of the finished laminate and may range in size from a 1/4 inch diameter wiring run cut to a 5 foot x 10 foot or larger opening in the main deck of the vessel. The larger cutouts would presumably be reinforced. However, the worst problem may arise because hull penetrations cannot be

fabricated totally crack free. The effect that small edge cracks have upon the engineering properties of the GRP laminate and the overall ship design elements may be a major area of concern, particularly considering the relatively low fracture toughness of typical GRP ship hull material as compared to ship steels.

The remaining chapters of this thesis are dedicated to understanding the various theoretical failure models and the correlation between experimental data and these theories.

CHAPTER 3

THEORETICAL MODELS OF FAILURE FOR GRP

In order to estimate the effect that a hull penetration and its associated cracks has on GRP laminate strength, several models which predict the performance degradation were evaluated. Each of the models addresses a through-the-thickness penetration in a 6 ply GRP laminate described in Table 4. The assumptions used in each model along with the limitations are presented. Detailed model development and calculations are provided in the corresponding appendices.

Notch Insensitivity Model

This model deals with a quasi-ductile material where a notch or crack is of no consequence in failure, beyond the reduction in cross-sectional area. In composites this behavior may result from widespread matrix cracking (damage zone) and crack tip blunting that occur at a crack site [13]. The remaining strength of the specimen, σ_{net}, is approximately the load averaged over the remaining cross sectional area. For the geometry presented in Figure 1, failure would occur at

$$\sigma_{net} = \frac{P}{t\,(w - 2a - D)} \qquad (1)$$

where P is the load at failure. In terms of the material tensile strength, σ_{uts}, the behavior is notch insensitive if

$$\sigma_{net} = \sigma_{uts} \qquad (2)$$

Appendix A presents calculations for various hole and crack sizes in a panel of typical GRP naval ship hull material using this model as the basis for calculations.

Stress Concentration Model

In this case failure is predicted by using the elastic stress concentration factor, K_T, for the hole, without considering edge cracks where present. K_T is defined as the ratio of the maximum stress in the presence of a geometric irregularity or discontinuity to the stress which would exist at the point if the irregularity were not present [14]. This relates to the failure stress as

$$\sigma_{failure} = \sigma_{uts} / K_{Torthotropic} \qquad (3)$$

In order to apply this model, the stress concentration present in an isotropic, finite width plate presented in Figure 2 is first calculated. Savin [15] has tabulated values of σ_θ/P along the contour of a circular hole for various values of $\lambda = a/b$. As expected, the most dangerous

stress concentration exists at the edge where $\theta = 90^{o}$. Appendix B presents calculations for the maximum isotropic stress concentration factors for various hole sizes as well as the expected or predicted failure stress for a typical GRP naval ship hull material.

The typical naval ship hull material is orthotropic, and so the effect of anisotropicity cannot be ignored. A correction factor, f, can be calculated by relating the orthotropic stress concentration factor for an infinite plate to the isotropic stress concentration factor for the same infinite plate. For the orthotropic infinite plate in Figure 3, the stress concentration factor is given by [16]:

$$K_{Torthotropic} = 1 + n\,(a/b) \qquad (4)$$

Since the circular hole is a special case where R=a=b, the stress concentration factor for an infinite plate with a circular hole becomes

$$K_{Torthotropic} = 1 + n \qquad (5)$$

where

$$n = \sqrt{2\left(\sqrt{\frac{E_y}{E_x}} - \nu_{xy} + \frac{E_y}{2G_{xy}}\right)} \qquad (6)$$

and E_x, E_y, G_{xy}, and ν_{yx} are the orthotropic elastic constants. For an isotropic material, n=2 and equation (4) becomes [16]:

$$K_{Tisotropic} = 1 + 2\,(a/b) \qquad (7)$$

and for the case with a circular hole

$$K_{Tisotropic} = 3 \qquad (8)$$

The effect that anisotropy has on the stress concentration for the geometry presented in Figure 3 can now be calculated. The correction factor f is used to correct the stress concentration factors presented in Appendix B. Appendix C contains the calculations for the correction factor and Table 5 presents the corrected stress concentration factor and predicted failure stress for the orthotropic material. The factor f for the material in question gives a stress concentration of about 15% higher than the isotropic case.

Linear Elastic Fracture Mechanics Model

In this model the material fails in a brittle fashion and the classical linear elastic fracture mechanics approach prevails. Fracture mechanics can be used to predict either the stress (σ) or crack size (a) required to fracture a particular sample. Broek [13] relates these two parameters

for the finite plate in Figure 4, with the stress-intensity factor K_I such that

$$K_I = \sigma \sqrt{\pi a}\, f(a/w) \qquad (9)$$

where w is the plate width.

K_I is a function of both specimen and crack geometry. In the case under consideration, the hull panel will be modeled as a flat rectangular sheet containing two edge cracks at a circular hole which is then subjected to uniform uniaxial tensile stress. This geometry is depicted in Figure 1. Given this geometry and loading scheme, a compendium of stress-intensity factors can be consulted for the K_I relationship [17]. Figure 5 presents the K_I/K_o relationship versus a/b for various R/b ratios and is accurate to within 1%. The K_I/K_o relation is used to correct the K_o value for the geometry considered by using it in

$$K_I = K_o\ (K_I/K_o) \qquad (10)$$

where

$$K_o = \sigma \sqrt{\pi a} \qquad (11)$$

Formula (10) is for an isotropic material and the subject material is an orthotropic GRP. However, earlier work has shown that orthotropic values differ by less than 25% [18] and the isotropic value is used here in the absence of an orthotropic analysis of the problem.

Failure, in the LEFM case, is defined to occur when the predicted stress-intensity factor (K_I) is greater than or equal to the critical stress-intensity factor K_Q, the material fracture toughness. The subscript Q used with K_Q indicates the candidate opening mode critical stress intensity factor as suggested by ASTM (E399), and is distinct from K_{Ic}, as the latter satisfies certain validity requirements which are not available yet for composites [19]. A K_Q value of 17.5 ksi(in)$^{1/2}$ is expected based upon K-calibration and test data for a similar E-glass fiber and polyester resin material [18]. However, a new value for the particular material in question has been determined using the test geometry in Reference 18.

CHAPTER 4

MATERIAL AND TEST METHODS

Material

In order to evaluate each of the failure models and select the one that best represents actual material failure, numerous tests were conducted on a candidate material. The material selection process was simplified by the fact that the only GRP naval ship hull under construction in the United States was the MSH. The test samples selected were actual panels of this hull material. The test panels were fabricated at Bell Aerospace Corporation's MSH production facility in New Orleans, Louisiana and shipped to MIT for analysis. The panel dimensions were 48 *inches* x 15 *inches* x 6 *ply* (.3125 in. nominal thickness) and were designed to have the material properties reported in Table 4.

Test Methods

The first test method concerned the effect of holes, both with and without notches, on the strength of large GRP panels. A series of 16 panels, 48 in. x 15 in., each with a central cutout, were tested under tensile load to failure. Ten of the panels had holes without edge cracks and 6 of the panels had holes with machined edge cracks. Table 6 tabulates the test specimen characteristics and the method used to cut the central hole.

Specimens were loaded in the specially designed and fabricated grip system shown in Figure 6. The grip was designed to transfer the tensile load to the specimen using pin loading. Each grip consisted of two 3/4-inch thick 4340 heat treated steel plates. Each plate was bored to receive a 1-1/8 inch pin and fifteen-5/8 inch grade 8 bolts through which the load was transferred to the specimen.

The GRP samples were drilled with a carbide tipped drill to enable them to accept the fifteen-5/8 inch bolts. An aluminum drill jig with RC 60 drill bushings provided the means by which precise hole alignment was maintained. Each specimen was then fit between the plates, bolted together and torqued to 50 ft-lbf. Figure 6 presents the plan for the grip plates and Figures 7 and 8 show a specimen bolted in the test apparatus. Figure 9 is the 600,000 lb electro hydraulic screw machine at the U. S. Army Materials Technology Laboratory in Watertown, Massachusetts that was used in testing the samples.

A chief concern in this test was obtaining a uniform load distribution across the entire sample width. By design, the applied load at the 1-1/8 inch pin was required to be transferred to the sample by the 15 bolts. This was verified by monitoring the strains at four equidistant points across the width of the sample. Strains up to 0.5% were measured and an even strain distribution was observed

across the sample. Figure 10 is a load-strain curve for the four strain gages.

The second test method utilized the same grip system but measured the ultimate tensile strength of a large specimen. Three full size test panels were machined to the specimen shape indicated in Figure 11 using a fine-toothed diamond bladed band saw. The shape of this specimen was determined to give the highest stress at failure without breaking in the grips [19]. In this test as well as the first a 600,000 lbf Baldwin electrohydraulic screw type universal testing machine was used, with a load rate of 6000 lbf/minute. Laboratory temperature and humidity were used in all tests unless otherwise noted.

The third test was a conventional tensile test using the specimen shape in Figure 12 [19]. Six samples, three cut vertically and three cut horizontally from full size panels, were machined to this shape using a diamond-edged wheel and a TensilKut router. Sample strain was measured during this test using an extensometer which allowed the bulk modulus of the samples to be determined. An Instron universal testing machine was used for this test, with a displacement rate of 0.05 inches/minute.

Finally, a conventional fracture mechanics test method was employed to determine the fracture toughness of the material. Six specimens, three cut vertically and three horizontally from full size panels, were machined to the

shape in Figure 13, from Reference 18. For the cleavage specimen the isotropic value of K_Q is given in [20] as:

$$K_Q = \frac{2\sqrt{3}\,P}{B\,H^{1/2}}\left(\frac{C}{H} + 0.69\right) \qquad (12)$$

where

P = applied load at fracture

B = thickness of specimen

H = half width of specimen

C = crack length

For the specimen shown in Figure 13, Equation (12) reduces to

$$K_Q = P\,(\,6.03C + 6.24) \qquad (13)$$

The geometry used in this specimen permits this test to only approximate the stress intensity factor due to free end effects. Data from this type of test has been in good agreement with finite element data given by Kanninen [21] for the specimen size and crack lengths of interest in this test. However, a more accurate value for K_Q can be obtained using the K-calibration data for a very similar E-glass/polyester material reported in Reference 18. Table 9 presents both values for K_Q.

The procedure for measuring the fracture toughness was to load the specimen until fracture occurred at the precut notch. The maximum load at fracture was recorded and

provided linearity was maintained in the load-deflection curve until the fracture point, this maximum load value can be used to calculate K_Q. This procedure is repeated a number of times by increasing the deflection in order to keep the crack moving. This provides a number of data points although the load to cause initial crack extension was used in calculating K_Q for each specimen. An Instron universal testing machine with a displacement rate of 0.05 inches/minute was used in this test.

Finally, the effect on strength due to hole machining method was evaluated. Two of the 5.0 inch specimen holes were machined with an ordinary arbor mounted hole saw while four others were machined with a carbide tipped parting tool mounted in a flycutter.

CHAPTER 5

DISCUSSION OF RESULTS

The results of the full scale tensile tests and the characteristics of the 19 large panels are presented in Table 7. Tables 8 and 9 present the results of the conventional tensile and fracture toughness tests. These experimental data are used to evaluate each of the three theoretical failure models discussed in Chapter Three. From this evaluation appropriate models are selected as best representing actual material failure.

Notch Insensitivity

The notch insensitivity model can be evaluated by calculating the degree of notch sensitivity displayed by the GRP. A good measure of this is the ratio of the strength of the remaining material, σ_{net}, from Equation (1), to the ultimate tensile strength of the material, σ_{uts}. A value of 1.0 would indicate notch insensitivity, while decreasing values less than 1.0 would indicate an increasing degree of notch sensitivity. Figure 14 shows one of the failed panels complete with machined crack and 5.0 inch hole. The average values of σ_{net} for each hole diameter, notch length and machining method tested were compared to the average tensile stress of the three full size tensile coupons. Figure 15

gives these data as a function of hole diameter plus notch length and shows that the material is strongly notch sensitive in all cases. When edge notches are present, the behavior is more notch sensitive. The data do not cover a sufficient range of specimen sizes to show the expected increase in notch sensitivity with hole or notch size. These data also show that the failure loads measured for the two machining methods varied by 5.67%, with the hole saw method exhibiting the higher load values. The difference is not great enough to draw a definitive conclusion. However, it suggests that the machining method does not have a great effect on strength. These results indicate that the notch sensitivity model is inappropriate as a model for failure in this material, and would be very non-conservative.

Stress Concentration

The applicability of the stress concentration model can be evaluated by comparing the actual failure stresses measured in the test specimens to the predicted failure stress from the model. The actual failure stress in the specimens is taken as the far field stress at the failure load as

$$\sigma_{failure} = \frac{P}{t \times W} \qquad (14)$$

where P = failure load

t = nominal specimen thickness of .3215 in.

W = nominal specimen width of 15 in.

The predicted failure stresses for the hole diameters used in the tests have already been reported in Table 5. Figure 16 shows a failed panel with a 5.0 inch diameter hole.

A reasonable measure of the validity of the stress concentration model is the ratio of the predicted failure stress to the actual failure stress, with the model becoming more accurate as the ratio approaches 1.0. Table 10 presents the data by which this model may be evaluated. When the raw data were compared, this model seemed to be inappropriate for predicting the failure strength due to the low values of the ratio. However, a more careful review of the data was pursued. Figure 17 gives the ratio of predicted to actual failure stress against hole diameter and shows that for holes greater than 10 inches in diameter the model approaches validity, following a consistent trend. This trend may be explained by the fact that in very large holes the volume of highly stressed material more closely approaches the volume of stressed material present in ultimate tensile strength specimens. This is significant because the value from the ultimate tensile strength specimen is used in the stress concentration prediction, therefore, as the stressed material volumes converge the model becomes more accurate.

Figure 18 shows both the predicted and experimentally measured failure stresses plotted against hole diameter. The plot shows that the predicted and experimental trends are similar, but that the predicted strength based on the ultimate tensile strength tests is lower. The difference in strength values may be explained by a magnification factor, which implies that the in-situ ultimate tensile strength at the hole is higher than in a standard tensile test; an effect that is apparently due to the smaller material volume and the constraint that exists around the failure site, as compared with an ultimate tensile strength specimen with a narrow gage section (although the local strength at the hole cannot readily be measured experimentally). If this is the case, an increased ultimate tensile strength value is necessary before the predicted failure stress is in agreement with the experimental data. For the values reported in Table 10, the local strength must be approximately 1.58 times the measured ultimate tensile strength in the large tensile specimens. For the material tested, this would require an in-situ strength of 41,000 psi at the hole edge, a value which can be considered conceptually sound and of reasonable magnitude. As shown in Figure 18, the predicted trend with hole size using the higher ultimate tensile strength value is in good agreement with the experimental data for all hole sizes.

This model is not sufficiently accurate for predicting the failure strength of the material and geometry under consideration, based on the measured ultimate tensile strength. However, the stress concentration model does appear to be theoretically correct based on the trend of the data, if a more representative in-situ strength value is used. If the measured ultimate tensile strength is used, it represents a conservative method for predicting failure strength and may be of use in predicting failure for relatively large hole diameters. However, the method does not apply to either holes with edge cracks or small holes where the hole size is similar to the damage zone size, which is on the order of one inch for this material (Figures 14, 16 and 19).

Linear Elastic Fracture Mechanics

The linear elastic fracture mechanics model can be evaluated by comparing the value of the stress intensity factor K_I at failure predicted by the model with the experimentally measured value of K_Q. Using the technique described in Chapter three, the value of K_I for each unique crack length is calculated at the failure load. Appendix D presents a sample calculation and the K_I values for the 6 panels with edge cracks that were tested. These values can now be compared with the experimentally derived value of K_Q (using an orthotropic K-calibration) that has been reported

in Table 9. Figure 19 shows a double-cantilever beam specimen, complete with crack propagation, used in evaluating K_Q. The longitudinal K_Q values in Table 9 are slightly higher than the calculated K_I at failure for the holes with notches (Appendix D).

Figure 20 gives the results of the six test specimens reported in Table 9 and indicates that the value of load necessary for crack extension is consistent with a constant K_Q criterion using the analytic K-calibration of Reference 18, over a broad range of crack lengths. The same K-calibration was used for tests conducted in both directions. However, they are only strictly valid for elastic constants with a load in the longitudinal direction (parallel to the long side of the panel). With the experimental values for K_Q established, the applicability of the linear elastic fracture mechanics model to holes with notches may be evaluated. The average K_Q values were 25.9 $ksi(in)^{1/2}$ loaded longitudinally and 28.0 loaded transversely.

Figure 21 compares the failure stress predicted using K_Q = 25.9 $ksi(in)^{1/2}$ with the experimental data for the 5 inch diameter hole with different notch sizes. The predicted failure stress is approached as the notch length becomes longer. This type of behavior is to be expected in this material because the damage zone size is of similar magnitude to the notch length, and precise modeling of short

cracks requires a two-parameter model [19]. It should also be noted that the hole with notches calculation is based on isotropic properties, which could also lead to the small differences shown in Figure 21 [18]. The significance of the model relies upon the fact that the predictions are reasonably close but non-conservative, falling above the experimental data. This model is considered valid but slightly non-conservative and therefore appropriate for predicting the failure strength of the GRP panels under investigation when edge notches are present or assumed at the cutout boundary, if the assumed K_Q is reduced slightly to provide a conservative prediction.

Ship Hull Design Strength

The application of any model that predicts failure must be considered in conjunction with the other major factors which influence strength. In the case of GRP for naval ship hulls the predictions made using stress concentration or linear elastic fracture mechanics must be considered in the context of effects of both ship hull strength and fatigue in seawater.

Fatigue studies for ships have chiefly concerned themselves with the maximum number of cycles a vessel will see at a particular stress level [23]. The area of most concern has been the maximum stress that a ship encounters in storm seas. Because of the lack of specific knowledge

concerning the size of storm waves to be expected at sea it has long been usual practice to design ships by assuming them to be poised on a stationary standard trochoidal wave [24]. The standard wave height used by both Lloyds Register and the U. S. Navy is $1.1(L)^{1/2}$, where L is the overall ship length. From this wave height a maximum bending moment and corresponding maximum ship structural stress can be calculated for a given hull geometry and thickness. This value is then subjected to a factor of safety for the specific material and load application used in the hull, and a maximum design stress for the material is obtained. Thomas and Cable evaluated a ship hull structure similar to the MSH and report a maximum stress of 2970 psi, which corresponds to the maximum bending moment load on the standard wave [11]. This conventional bending moment calculation ignores the dynamic effects of the ship's motion. The most deleterious motion results from slamming, (the impact of the hull on the water during a large downward pitch). In naval vessels slamming stresses of a magnitude 1.6 times the primary stress have been recorded [24]. It is therefore reasonable to assume that the MSH type hull would see stresses 1.6 times 2970 psi or 4700 psi.

Fatigue Effects in Seawater

The fatigue of GRP in a seawater environment is a major concern. Investigators using a similar material to that

used here have found that the stress which can be withstood decreases by about 11.6% of the ultimate tensile strength per decade of cycles when subjected to a sinusoidal load-time curve between a maximum tensile load and a minimum load which was approximately 5% of the maximum [26]. Figure 22 reproduces these data. These results are applied to the ultimate tensile strength of the typical GRP ship hull material reported in Table 4. Figure 23 shows an equivalent loss of strength per decade for an initial ultimate tensile strength of 26,000 psi. The number of cycles to the extreme sea state slamming stress of 4700 psi which could be withstood by this material is calculated as 10^7, a value unlikely to be seen in any ship hulls. This treatment assumes that the material exhibits ideal mechanical properties and that any cutouts present have been adequately reinforced. However, this may not be the case since many unreinforced holes could exist in the ship hull.

Stress concentration theory can be used to predict the failure point for a cutout that is exposed to cyclic loading. The predicted failure stress for a particular hole size is calculated by applying the stress concentration factor to the ultimate tensile strength and then reducing that value for each fatigue cycle. Any applied stress levels above these predicted stresses will cause failure. Figure 24 presents these data for two hole sizes as a function of stress and number of cycles. The plot shows

that for slamming stresses of 4700 psi a 7.5 inch unreinforced hole will fail after 10 cycles and that in seas without slamming 10,000 cycles will cause failure. This model provides an alarming result that warrants a further review of fatigue using a fracture mechanics approach.

Linear elastic fracture mechanics can be applied to fatigue in notch sensitive woven fabric and chopped strand mat composites by studying the propagation of macroscopic cracks [27]. A mode of ligamented crack growth, by which crack initiation is defined at a notch as the first ligament failure, is used in this analysis. This method is most easily defined by a formula which predicts the number of cycles to crack initiation

$$\log N = \frac{\sigma_f}{S}(1 - K_I/K_Q) \qquad (15)$$

where

N = cycles to crack initiation

σ_f = ultimate tensile stress

S = slope of S-N curve

K_I = stress intensity factor at the applied stress

K_Q = fracture toughness

This method can be used to predict the number of cycles to crack initiation for the hull panels under study by using experimental values for K_Q and σ_f and a value of S from the slope of Figure 23. These values are in close agreement with the values used in Reference 26 and are compared in

Table 11. The values of K_I for each notch length and various applied stress levels are calculated by the method used in Appendix D. Figure 25 presents these data as a function of applied stress and number of cycles to crack initiation for different notch lengths and shows that the number of cycles to failure decreases directly with increasing notch length. This plot is significant because once the first fibers are broken the crack propagation rate will increase significantly. This can be demonstrated by using the fatigue crack growth rate law [27]

$$dc/dN = d/\exp[\ 2.3\ \sigma_f/S(1 - K_I/K_Q)] \quad (16)$$

where d is the experimentally measured ligament width, which is assumed to be 0.125 in. based on measurements for a similar E-glass/polyester material in Reference 26. Figure 26 presents data from the crack growth rate law and shows the direct relationship between crack length and the crack growth rate. As the crack grows under a constant applied stress range, it accelerates rapidly. The analysis by fracture mechanics supports the findings of the stress concentration model which concluded that fatigue is a major determinant in the failure equation for a stressed GRP panel with cutouts and edge cracks.

The use of high factors of safety in GRP ship design has precedent [28] and would be of benefit in reducing the chance of catastrophic failure in the hull. The findings in

this paper indicate that three conditions directly affect material strength and should be considered in determining factors of safety. Saltwater exposure, fatigue, and the presence of stress concentrations directly impact on the strength and are of primary concern. Figure 27 presents a simplified model to illustrate the components of a total factor of safety. The factors shown in Figure 27 include: (1) The effect of sea water on the strength, about 12.9% from Reference 26. (2) The effect of fatigue (in sea water) of 11.6% per decade of cycles from Reference 26. The safety factor needed for various sea conditions, related to the expected number of cycles at a given maximum stress level can be assigned and used to account for the effects of fatigue. (3) The effect of stress concentration at unreinforced holes or other geometrical irregularities. The factors shown represent both the theoretical predicted stress concentration based on the measured ultimate tensile strength, and a lower factor which represents the actual experimental data. (4) Other factors which have not been addressed in this study, including statistical variations in material properties, flaws in fabrication, elevated temperatures, impact, etc..

The results shown in Figure 27 clearly indicate two areas which are critical in reducing the required safety factors. First, the reinforcement of holes and improved design and analysis procedures for other geometrical

irregularities. Second, the ability to operate in fatigue at higher stresses, either by improving the fatigue resistance or by raising the initial strength while maintaining a similar relative S-N curve slope. Graphite fiber reinforcement would improve the fatigue resistance (as well as the stiffness), while S-glass would raise the initial strength at a much lower cost than graphite.

CHAPTER 6

CONCLUSIONS AND RECOMMENDATIONS

The objective of this thesis was to help solve a practical, real world problem: to assess the effects of cutouts on GRP ship hull performance. The approach was to combine theoretical modeling and an experimental test program with specimens of appropriately large size. The scope precluded the analysis of many associated factors, but the results resolve a specific portion of the technology gap in fracture mechanics reported in Reference [1].

Conclusions

The experiments conducted in this study provide data from which appropriate theoretical models for determining the failure strength of GRP hull panels can be selected. Test methods were developed for full scale tensile tests on 16 large panels, 48 in. x 15 in., each with a central cutout. Ten of the panels had holes without edge cracks and six of the panels had holes with machined edge cracks. Two associated test methods, a standard tensile test and a conventional fracture toughness test, were conducted on a number of the remaining hull panels. All test data were then used for validation assessment of three theoretical models.

The notch sensitivity was evaluated by comparing the ratio of the net strength of the remaining cross sectional area to the tensile strength for panels with central holes, with and without machined edge notches. All ratios were much less than 1.0 indicating that the material is notch sensitive, so that a model which includes stress concentration effects is required.

A stress concentration model was evaluated by comparing the experimental failure stress in the 10 panels with simple holes to the predicted failure stress, calculated using the measured ultimate tensile strength of the material and the orthotropic stress concentration factor for the particular hole size. This model appears to be valid based on the trend of the data, but an accurate prediction requires a local strength at the hole which is somewhat higher than that measured from the standard tensile tests.

For holes with edge notches, a linear elastic fracture mechanics model was evaluated by comparing the experimentally applied stress at failure with that predicted from the fracture toughness. The predicted values were close to the experimental results, but were slightly non-conservative. The fracture mechanics model appears to be valid if notches of 1/4-inch or greater length are present at the edge of the hole. Discrepancies between measured and predicted failure stresses may be due to the

isotropic analysis used and/or the large damage zone at the notch tip.

The additional influence of hull strength design practices, sea water environments, and fatigue cycling were evaluated by reference to other studies in the literature. Of particular importance was the effect of material fatigue when combined with the results for cutouts. To avoid the need for very high safety factors, cutouts in the size range studied here must be fully reinforced to eliminate their stress concentrating effect.

In summary, the need for high factors of safety and the requirement to reinforce large holes are two sound engineering practices which this research advises in using GRP for naval ship hulls.

Recommendations

In concluding this thesis, the following recommendations are summarized to provide direction for continued research in the development of sound models for failure analysis in GRP hulls.

- Development of a method by which the in-situ strength at a hole boundary may be measured or predicted

- Development of a series of guidelines for reinforcing hull penetrations in GRP ships, and assessment of the minimum hole size which requires reinforcement.

- Investigation of the effect of different methods of machining cutouts on laminate strength.

- Full scale tensile tests on a large sandwich panel with cutouts

- Development of methods by which defects at cutout boundaries may be repaired.

- Development of a set of guidelines for inspecting hull penetrations.

- Development of a set of acoustic emission guideline data for sandwich panels with hull cutouts. Examination of the applicability of continuous in-service acoustic emission monitoring at critical stress points in an actual hull, based on guideline data.

- Consideration of a more fatigue resistant composite such as graphite/epoxy, or a higher initial strength material such as S-glass reinforcement, particularly in areas of high stresses. Further study is also needed of GRP in high cycle, low stress fatigue.

- Consideration of compressive loading effects.

REFERENCES

1. Dobyns,A.L., Zenker,G.C., Montgomery,M.O., and Critchfield,M.O., "Assessment of the Applicability of Fiber-Reinforced-Plastic (FRP) Analysis and Design Methods to Naval Ship Structures," David W. Taylor Naval Ship Research and Development Center Report 85-080, (September 1985), p. 112.

2. Pohler,C.H., Deppa,R.W., Corrado,J.A. and Graner,W.R., "Advanced Composite Structures for High Performance Ships," Naval Engineers Journal, Volume 87, (April 1975), pp. 189-197.

3. Noton, Bryan R., editor, Composite Materials: Volume Three, Engineering Applications of Composites, Academic Press, New York, 1974, p. 224.

4. Henton, D., "Glass Reinforced Plastics in the Royal Navy," Transactions of The Royal Institution of Naval Architects, Volume 109, (1967), p. 487.

5. "Reinforced Plastics Growth to Slacken in 1985," Chemical and Engineering News (February 4, 1985), p. 15.

6. Lubin, George, editor, Handbook of Composites, Van Nostrand Reinhold Company, New York, 1982, p. 706.

7. Wendt, F.W., Leibowitz, H., and Perrone,N., editors, Mechanics of Composite Materials, Proceedings of the Fifth Symposium on Naval Structural Mechanics, Pergamon Press, New York, 1970, p. 79.

8. Spaulding, K.B., "Fiberglass Boats in Naval Service," Naval Engineers Journal, Volume 78, (April 1966), pp. 333-340.

9. Dixon,R.H., Ramsey,B.W. and Usher,P.J., "Design and build of the GRP Hull of HMS WILTON", Symposium on GRP Ship Construction, Royal Institution of Naval Architects, London, 1973, p.1.

10. Thomas, R.D., Cable, C.W., and Mette, J.A., "Feasibility Design Report for an Advanced Mine Warfare Ship (MWSX)", unpublished MIT report dated May 1985.

11. Thomas, R. D. and Cable, C. W., "Quality Assessment of Glass Reinforced Plastic Ship Hulls in Naval Applications," Ocean Engineer's Thesis, MIT Dept of Ocean Engr. (1985), pp. 12-62.

12. Crane, R.M., and Macander, A.B., "Flaw Criticality and Nondestructive Assessment of Advanced Composite Pressure Hulls," David W. Taylor Naval Ship Research and Development Center Report 84-010, (May 1984), p. 69.

13. Broek, D., Elementary Engineering Fracture Mechanics, Martinus Nijhoff Publishers, Boston, 1982, p. 38.

14. Crandahl, S. H., Dahl, N. C. and Lardner, T. J., An Introduction to the Mechanics of Solids, McGraw-Hill Book Company, New York, 1978, p. 302.

15. Savin, G. N., Stress Concentration Around Holes, Pergamon Press, New York, 1961, p. 109.

16. Whitney, J. M., Daniel, I. M. and Pipes, R. B., Experimental Mechanics of Fiber Reinforced Composite Materials, Society for Experimental Stress Analysis, Brookfield Center, 1982, p. 49.

17. Rooke, D. P. and Cartwright, D. J., Compendium of Stress Intensity Factors, Her Majesty's Stationary Office, London, 1976, p. 159.

18. Mandell, J. F., McGarry, F. J., Wang, S. S. and Im, J., "Stress Intensity Factors for Anisotropic Fracture Test Specimens of Several Geomtries," Journal of Composite Materials, Volume 8, (1974), p.106.

19. Mandell, J. F., McGarry, F. J., Kashihara, R. and Bishop, W. O., "Engineering Aspects of Fracture Toughness: Fiber Reinforced Laminates," MIT Research Report R73-54, 1973, p.4.

20. Srawley, J. E. and Gross, B., "Stress Intensity Factors for Crackline-Loaded Edge-Crack Specimens," Materials Research and Standards, Volume 10, (1967), pp. 155-162.

21. Kanninen, M. F. and Popelar, C. H., Advanced Fracture Mechanics, Oxford University Press, New York, 1985, p. 211.

22. Minesweeper Hunter (MSH-1) Class Ship Specification, Bell Aerospace Publication 7635-947004 Rev D of 31 May 1985.

23. Yuille, I. M., "Longitudinal Strength of Ships," Royal Institution of Naval Architects, London, 1962, p.69.

24. Comstock, J. P., editor, Principles of Naval Architecture, The Society of Naval Architects and Marine Engineers, New York, 1967, p. 174.

25. Design Data Sheet 100-5, U. S. Naval Sea Systems Command, Washington.

26. Mandell, J.F., McGarry, F.J., Barton, W.D., and Demchick, R.P., "Effect of Water on the Crack Propagation Rate in Fiberglass Laminates Under Static and Dynamic Loading," Proceedings of the 31st Annual Technical Conference, Reinforced Plastics/Composites Institute, The Society of the Plastics Industry, Washington, 1976.

27. Pritchard, G., editor, Developments in Reinforced Plastics, Volume 2: Properties of Laminates, Applied Science Publishers LTD, Essex, 1982, pp. 93-98.

28. Sjogren, J., Celsing, C.G., Olsson, K.A., Levander, C.G., and Hellbratt, S.E., "Swedish Development of MCMV Hull Design and Production", no date.

TABLE 1

Chief Advantages and Disadvantages of
Glass Reinforced Plastics in Naval Applications [4]

Advantages	Disadvantages
- High Strength/weight ratio	- Low elastic modulus
- The ability to fabricate large, complex shapes in one piece	- The differing elongations before failure of the two GRP constituents
- The ability to design directionally and therefore more economically	- The highly anisotropic nature of the material, in particular the relatively low ILSS available
- The comparative ease of forming complicated shapes	- The combustibility of the material
- The resistance to corrosion	- The relatively high material costs
- The resistance to marine biological attack	- The difficulty or indeed the impracticality of checking the quality and ensuring the uniformity of large fabricated structures
- The ease of maintenance and repair	- The possible deterioration due to long term immersion in sea water, particularly under conditions of high pressure and loading
- The fact that it is non-magnetic	- The initial mold costs, for small numbers
- The variation of mechanical properties within very wide limits	- The fall off in appearance after a period in service
- The fact that it does not warp, shrink or split	- The inherent difficulty in joining parts together
- With increasing use, future costs are likely to come down	
- The fact that it is radar and acoustically transparent	
- The fact that it has low thermal conductivity	
- The high degree of surface finish needs to be produced only on the mold surface	
- The ability to use sandwich material	

TABLE 2

Forecast of Demand for Reinforced Plastics, 1975-1985 [5]

Millions of lb	1985	1984	1983	1982	1981	1980	1975
Transportation, land	570	540	458	359	445	416	265
Construction	443	430	400	312	309	287	175
Anticorrosion	326	310	288	235	275	252	163
Marine	325	309	276	230	290	275	285
Electrical	205	189	170	140	178	162	82
Consumer goods	149	143	128	84	110	103	64
Appliance	130	123	106	82	112	104	64
Aircraft	35	29	25	22	28	25	24
Other	86	80	72	64	74	70	53
TOTAL	2269	2153	1923	1528	1821	1694	1175

Annual Change %	1984-1985	1983-1984	1980-1985	1975-1985
Transportation, land	5.6	17.9	6.5	8.0
Construction	3.0	7.5	9.1	9.7
Anticorrosion	5.2	7.6	5.3	7.2
Marine	5.2	12.0	3.4	1.3
Electrical	8.5	11.2	4.8	9.6
Consumer goods	4.2	11.7	7.7	8.8
Appliance	5.7	16.0	4.6	7.3
Aircraft	20.7	16.0	7.0	3.8
Other	7.5	11.1	4.2	5.0
TOTAL	5.4%	12.0%	6.0%	6.8%

TABLE 3

Existing Mine Warfare Ships with GRP Hulls [10]

Country	Class	Length (ft)	Displ. (tons)	Entered Service	Number Planned	Notes
Australia	Catamaran	101	160	Mid-80's	6	1
Belgium	Tripartite	154	544	80-87	10	2
France	Tripartite	154	544	80-87	15	2
Italy	Lerici	163	500	1983	10	3
Malayasia	Mahamiru	163	500	1984	4	3
Netherlands	Tripartite	154	544	80-87	15	2
Sweden	M80	155	340	1984	6	1
Britain	Wilton	152	450	1973	1	2
Britain	Hunt	197	725	1980	12	2
USSR	Zhenya	140	300	1970	3	-
USSR	Andryusha	147	360	1970	2	5
USSR	Sonya	160	460	1973	42	4
USA	MSH	150	434	1987	3	1

Notes:

1. GRP foam core sandwich
2. GRP single skin, stiffened
3. GRP single skin, monocoque
4. Wood with GRP sheath
5. GRP structure, unconfirmed

TABLE 4

GRP Naval Ship Hull Material Properties [22]

Hull material: combination of marine grade woven roving and chopped strand mat in a marine grade isophthalic polyester resin

Glass content: 45% + 3% by weight

Woven Roving: 18oz./yd^2

Chopped Strand: 9oz./yd^2

Minimum Mechanical Properties:

tensile strength	24,200 psi
tensile modulus	1.7×10^6 psi
flexural strength	38,000 psi
flexural modulus	1.7×10^6 psi
compressive strength	25,000psi
compressive modulus	1.9×10^6 psi
shear strength	14,000 psi
shear modulus	0.45×10^6 psi
ILSS	1.0×10^3 psi
Poisson's ratio	0.19

TABLE 5

Maximum Orthotropic Stress Concentration Factors and Predicted Applied Failure Stress as a Function of Hole Diameter

Hole Diameter(in)	$K_{Torthotropic}$	$\sigma^{*}_{failure(psi)}$
3.75	3.727	6975
5.00	3.998	6503
7.00	4.732	5494
7.50	4.954	5248

*assuming σ_{uts} = 26000 psi

TABLE 6

Full Size GRP Test Panel
Characteristics

Number of Samples	Hole Diameter	Crack Length	Machining Central Cutout
2	7.50	-	1
4	5.00	-	1
2	5.00	-	2
2	3.75	-	1
2	5.00	1.00	1
2	5.00	0.50	1
2	5.00	0.25	1

* 1. Carbide tipped parting tool mounted in a flycutter
2. Arbor mounted hole saw

TABLE 7

Characteristics of and Tensile Tests Results for Large GRP Panels

Panel Number	Hole Diameter(in)	Crack Length(in)	Failure Load(lbf)	σ_{net}
1	5.00	-	44560	14259
2	5.00	-	46990	15037
3	5.00	-	47540	15213
4	5.00	-	47260	15123
20	5.00	-	48240	15437
21	5.00	-	50530	16170
12	3.75	-	52470	14925
13	3.75	-	52870	15039
5	7.00	-	41260	16504
14	7.50	-	36940	15761
15	7.50	-	36300	15488
6	5.00	1.0	27350	10940
7	5.00	1.0	25080	10032
8	5.00	0.5	29980	10659
9	5.00	0.5	29320	10425
10	5.00	0.25	35030	11799
11	5.00	0.25	30980	10435
17	Full Size Tensile		23620	27485
18			22360	26937
19			18860	23552

TABLE 8

Conventional Tensile Test Results

Sample Number	Specimen Orientation	Failure Stress(psi)	Young's Modulus(psi)
22	Vertical	27554	-
23	Vertical	24960	1.62×10^6
24	Vertical	30933	1.84×10^6
25	Horizontal	32000	2.47×10^6
26	Horizontal	35520	2.42×10^6
27	Horizontal	35413	-

TABLE 9

Fracture Toughness Test Results

Sample Number	Specimen Orient.	Propagation Load (lbf)	Crack Length	Isotropic K_Q	Orthotropic K_Q
28	Vertical	1725	1.484	26.2	22.9
		1525	2.359	31.2	29.2
		1175	2.625	25.9	24.8
29	Vertical	1850	1.812	31.8	28.4
		1550	2.219	30.4	27.7
		1375	2.469	29.0	27.9
30	Vertical	1875	1.562	29.3	26.4
		1675	1.844	29.0	26.2
		1325	2.250	26.2	24.1
31	Horizontal	2175	1.360	31.4	27.8
32	Horizontal	2275	1.312	32.2	28.4
33	Horizontal	2175	1.375	31.6	27.8

TABLE 10

Stress Concentration Model Predicted
Stress Versus Measured Failure Stress

Hole Diameter(in)	σ_{pred}	σ_{fail}	Ratio
3.75	6976	11236	0.620
5.00	6514	10137	0.642
7.00	5489	8802	0.623
7.50	5246	7812	0.671

TABLE 11

Dynamic Fatigue Properties for
Woven Roving/Mat Laminates in Salt Water

	Reference [26]	Table 4
Measured σ_f (Ksi)	31.0	26.0
Extrapolated σ_f (Ksi)	27.0	22.6
S (Ksi/decade)	3.14	3.02
K_Q (Ksi in)	24.8	25.9
Ligament Width, d (in.)	.125	.125

FIGURE 1

Geometry for Notch Insensitivity Model

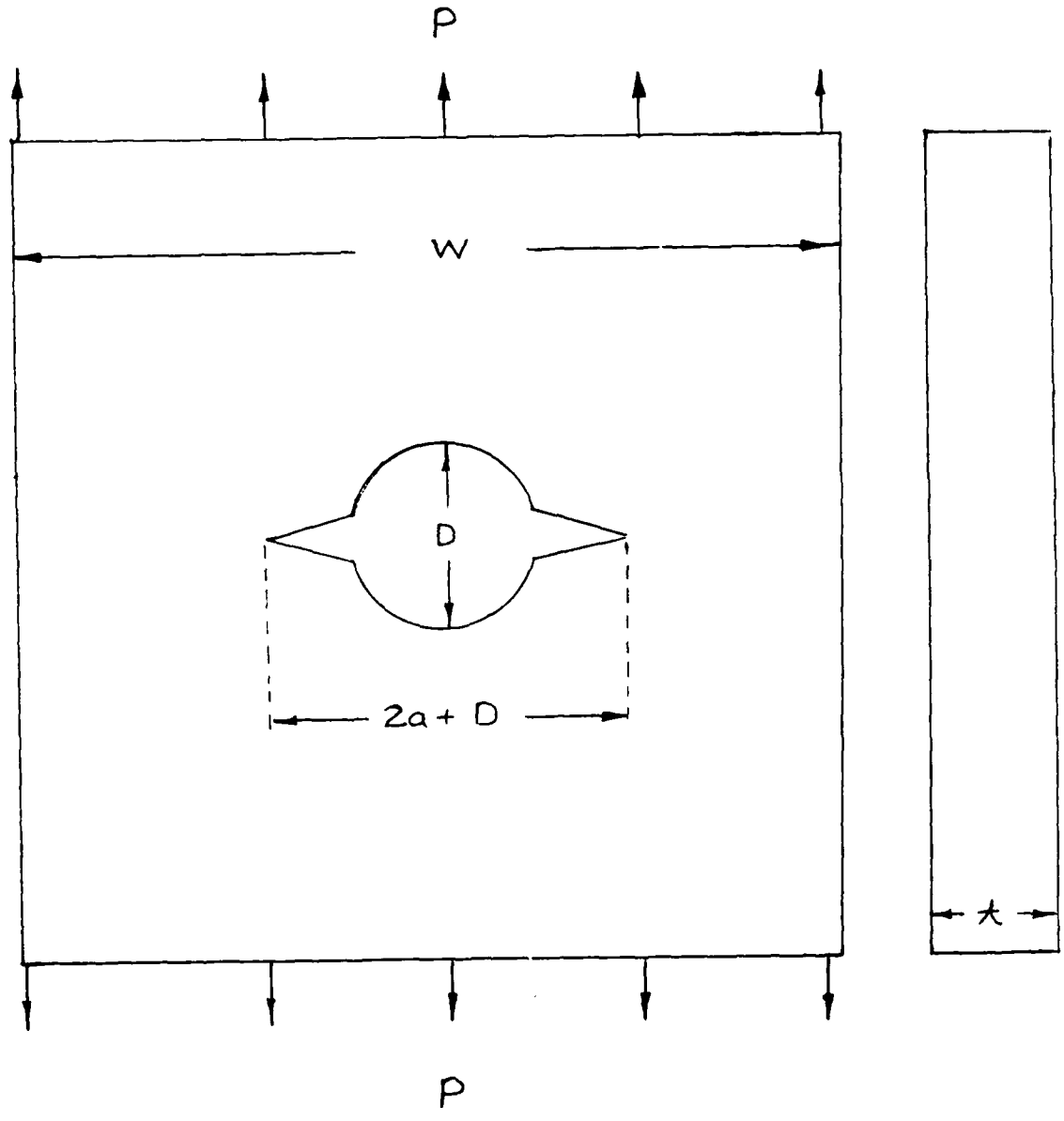

FIGURE 2

Isotropic Finite Width Plate

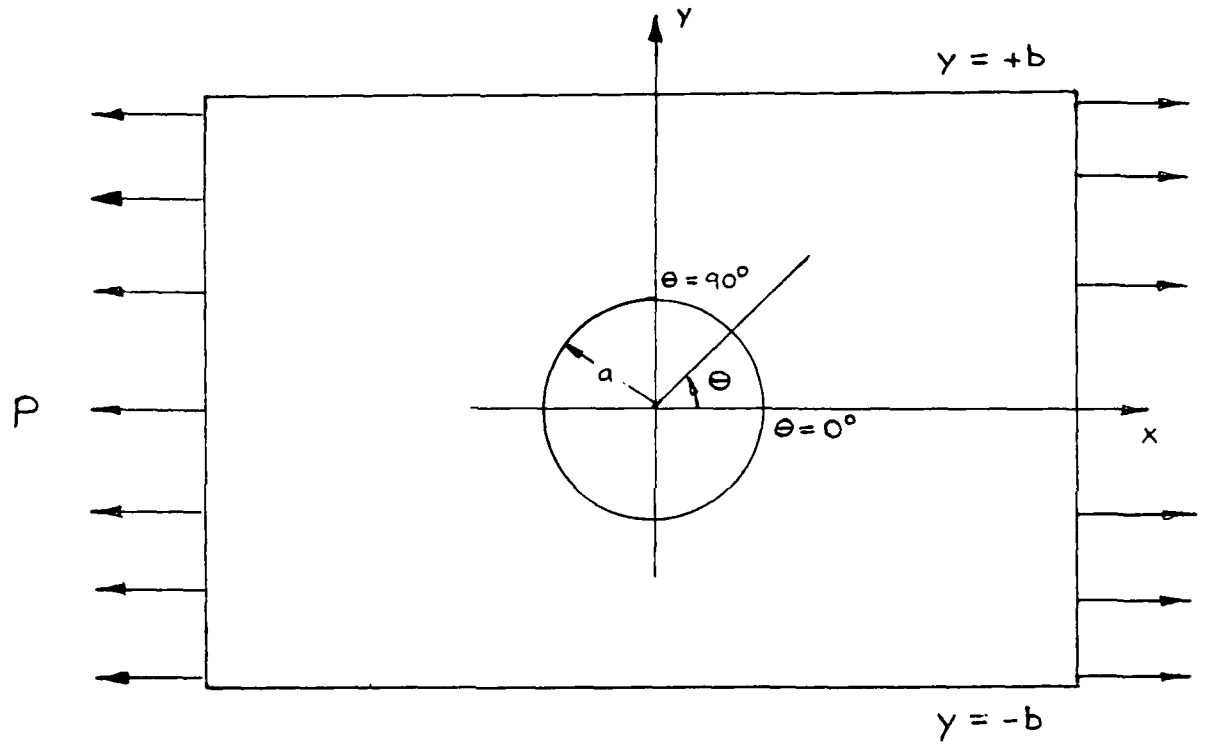

P = uniform tensile stress

a = hole radius

b = plate half width

$\lambda = a/b$

FIGURE 3

Orthotropic Infinite Plate

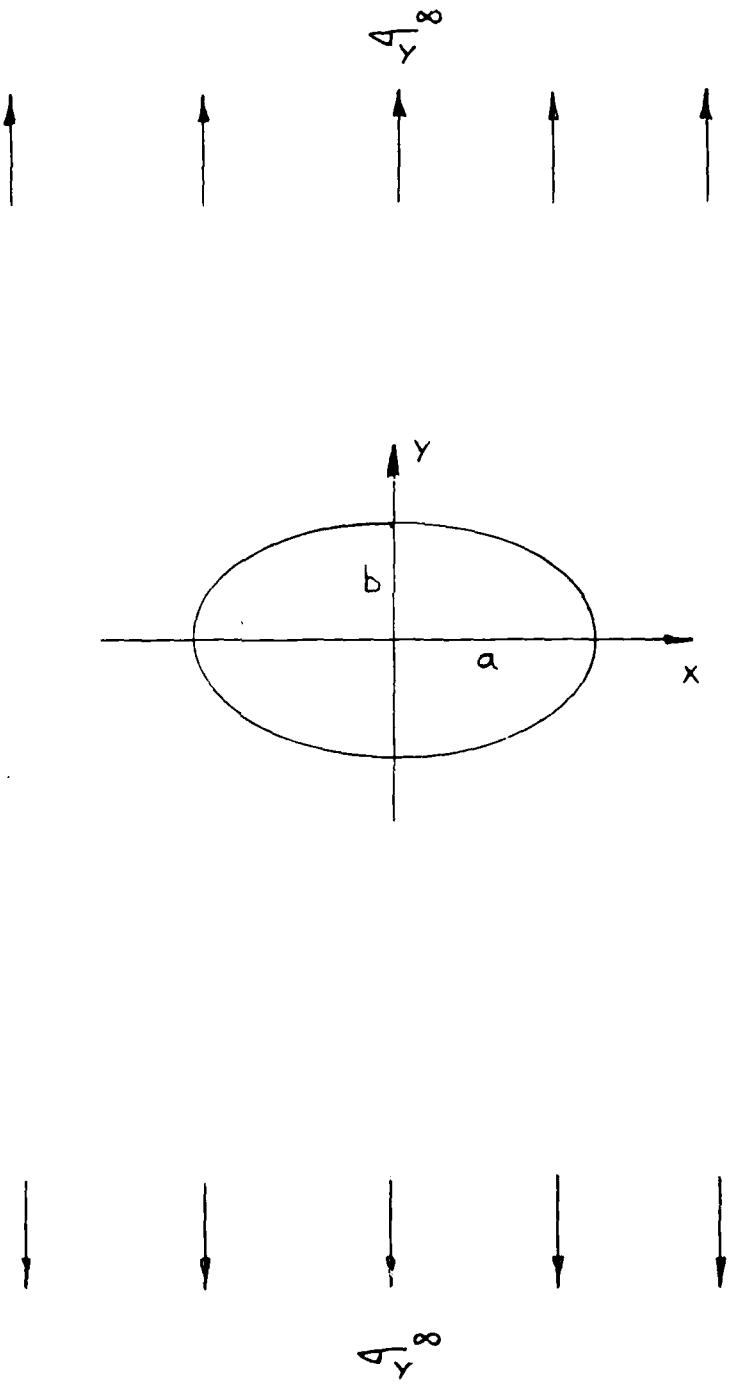

FIGURE 4

Finite Plate

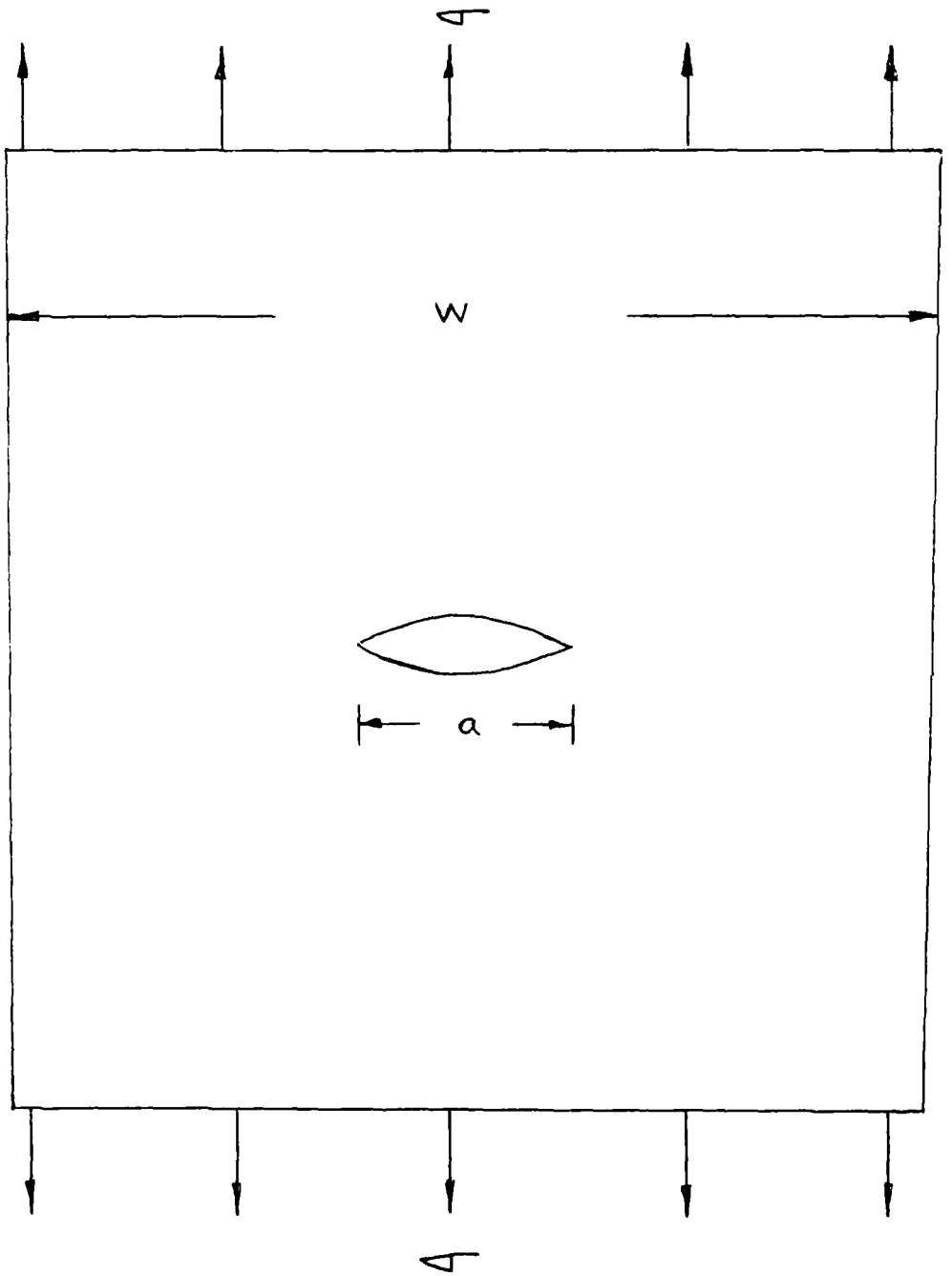

FIGURE 5

Stress Intensity Factor Graph for a Rectangular Plate with Two Edge Cracks at a Circular Hole (From [17])

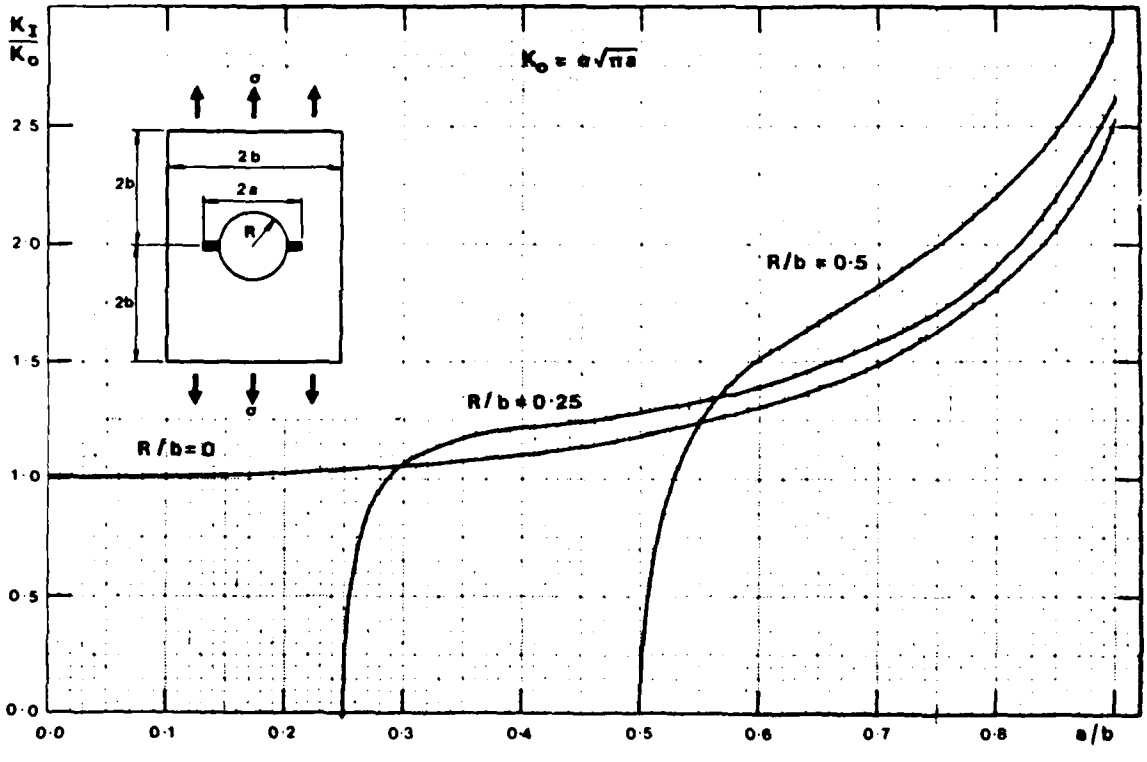

FIGURE 6

GRP Grip Half

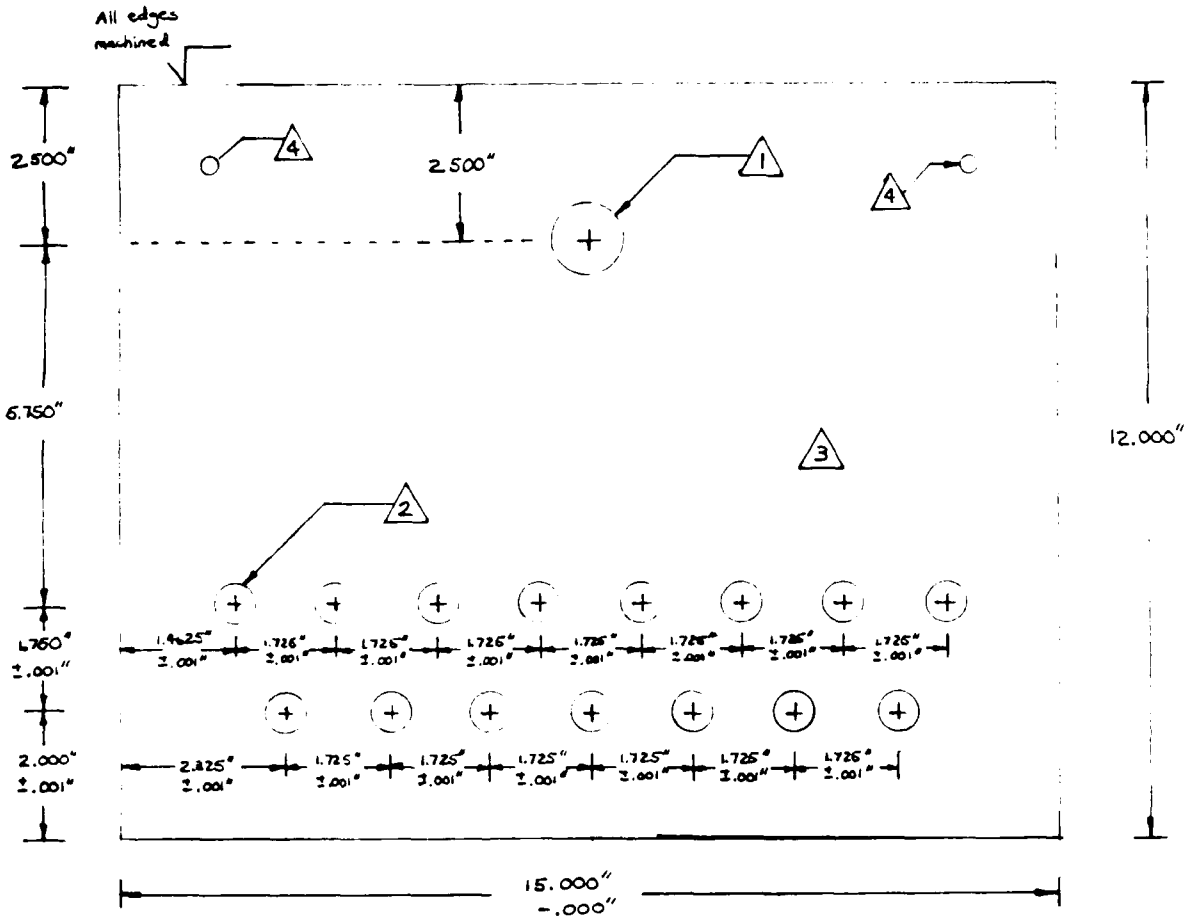

1. Bored/Drilled to 1.125" +.001" -.000"
2. Bored/Drilled to 0.625" +.010" -.000"
3. Heat treated 4340 Steel plate (RC 40) 3/4" thick

FIGURE 7

GRP Specimen in Grip

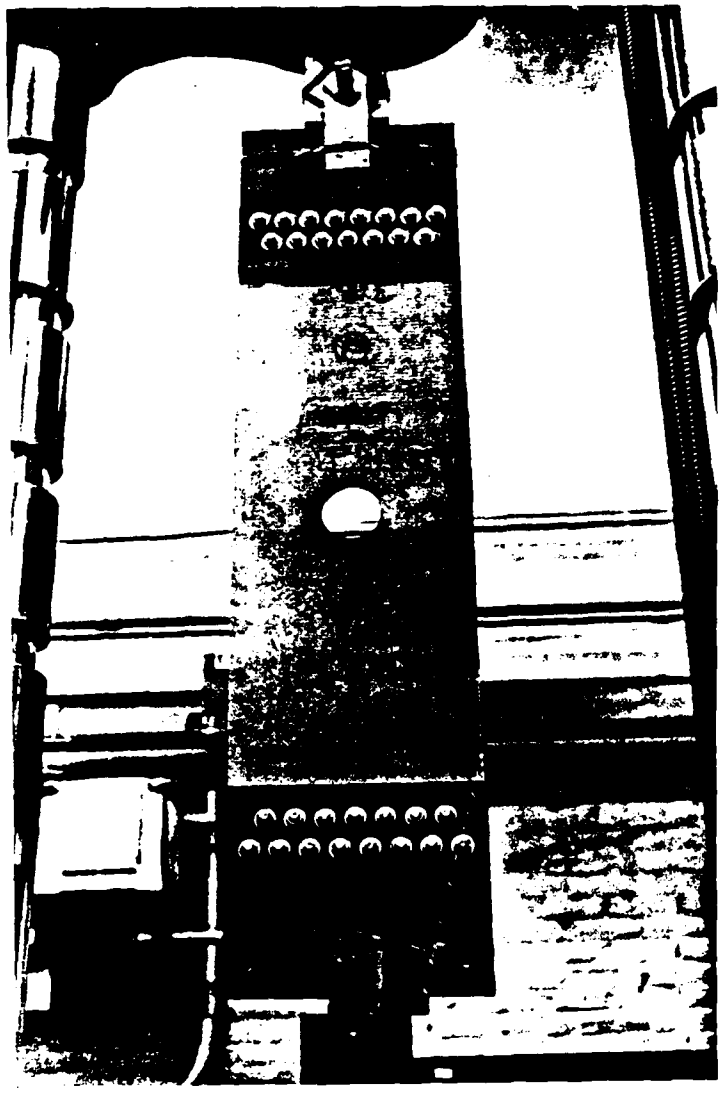

FIGURE 8

GRP Specimen and Grip
in Test Apparatus

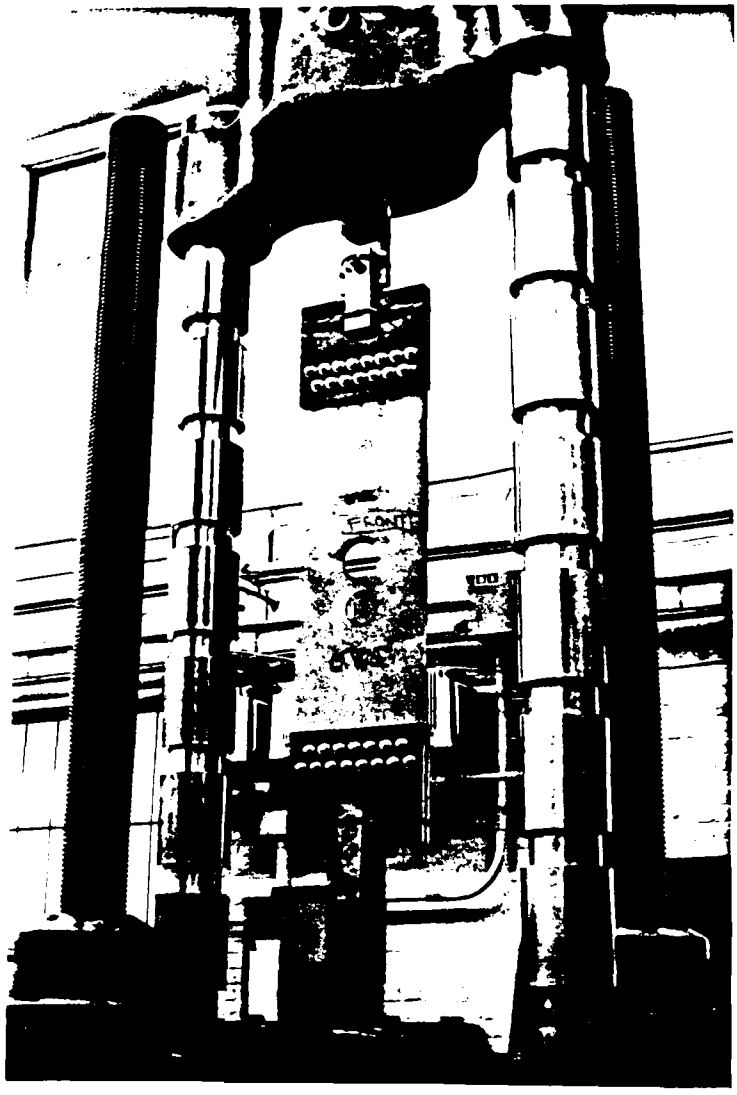

FIGURE 9

600,000 Lbf Test Apparatus

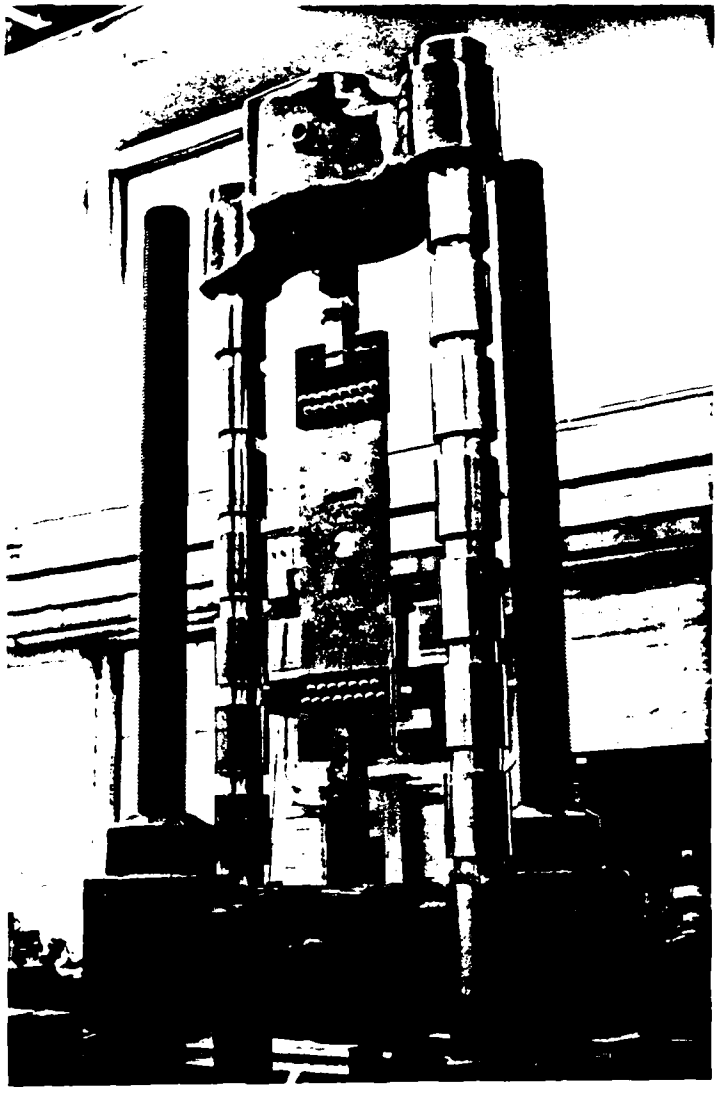

FIGURE 10

Load-Strain Curve
for Load Distribution

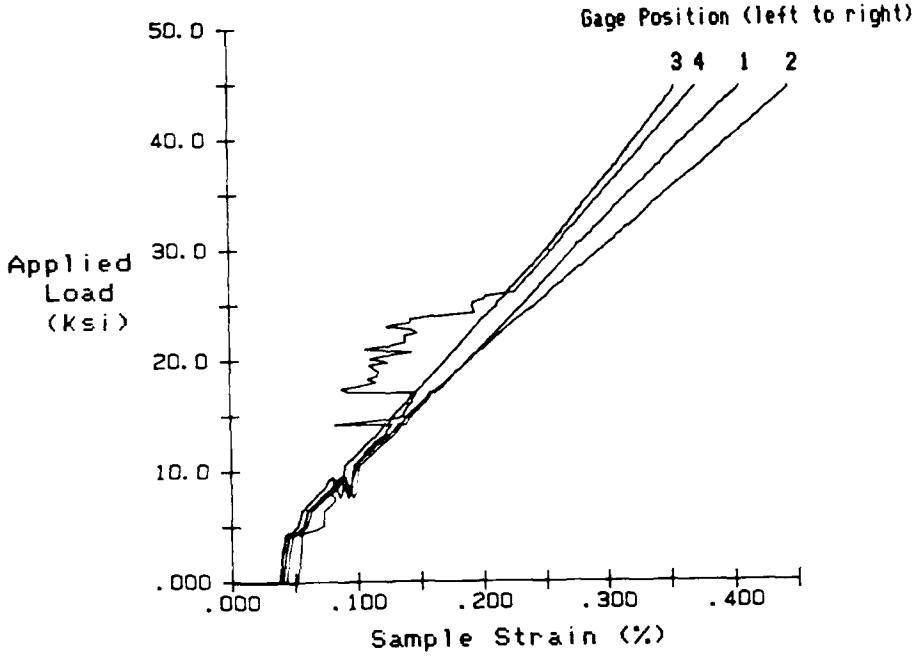

FIGURE 11

Large Unnotched Tension Specimen

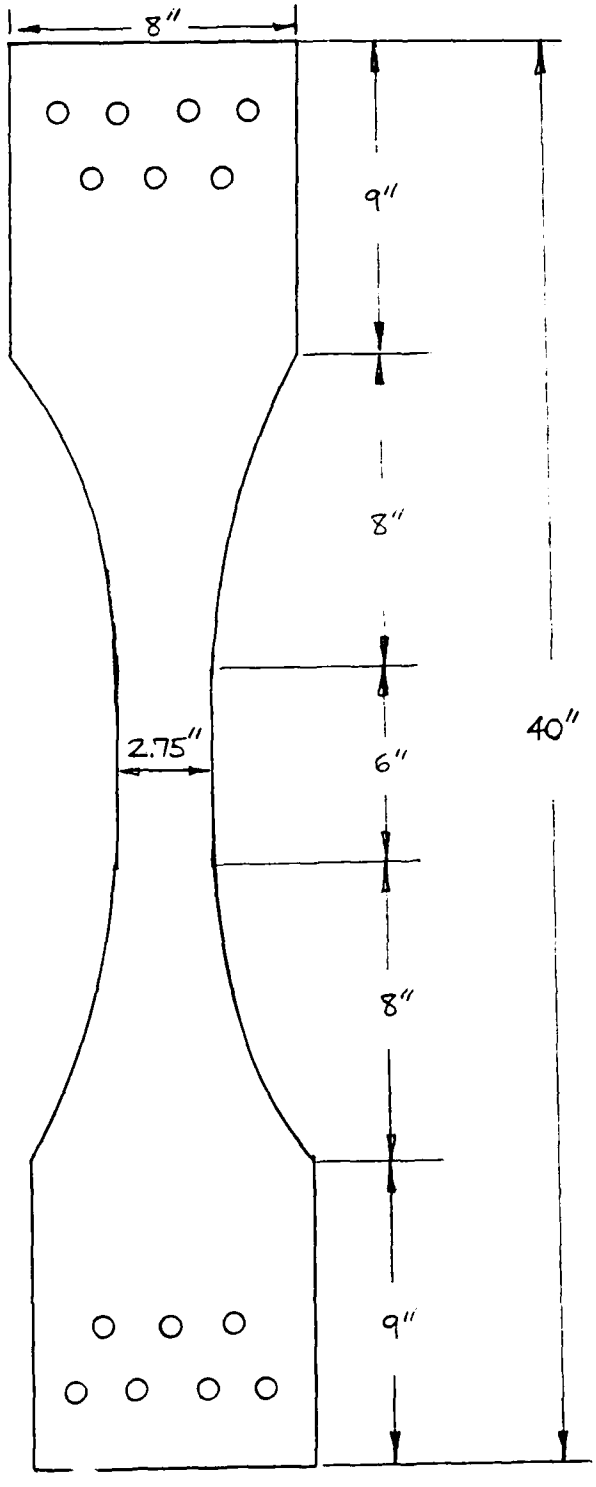

FIGURE 12

Standard Unnotched Tension Specimen [18]

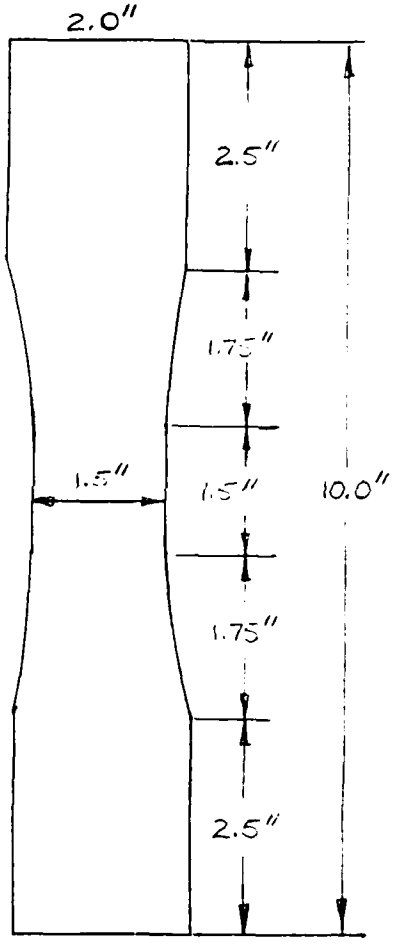

FIGURE 13

Double-Cantilever Beam Specimen [18]

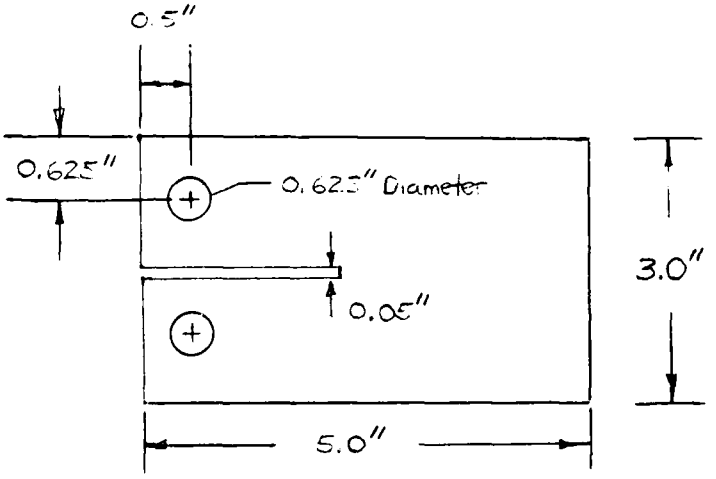

FIGURE 14

Failed Panel with Machined
Cracks at a 5.0 inch Hole

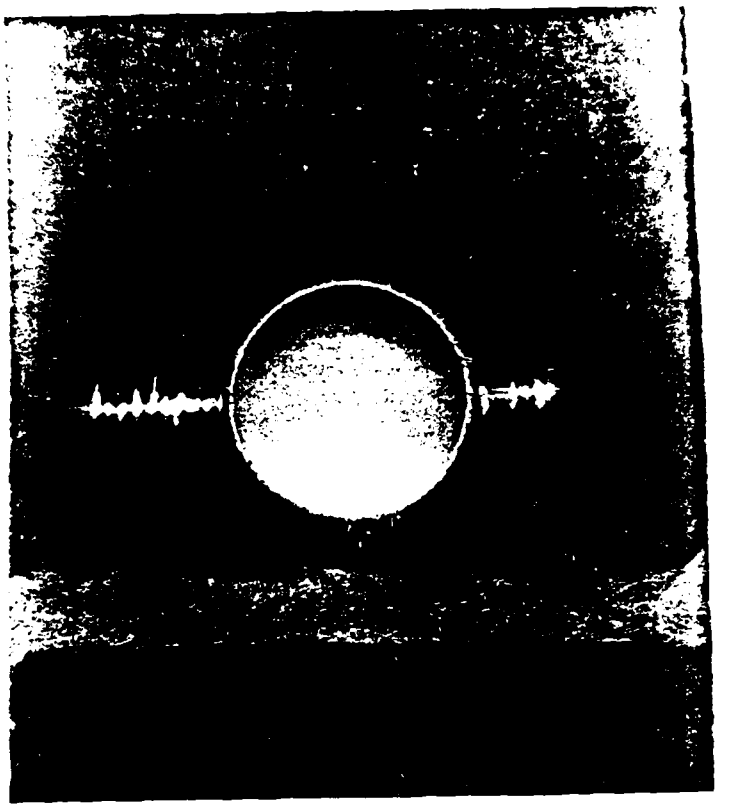

FIGURE 15

Notch Sensitivity as a Function
of Hole Diameter plus Notch Length

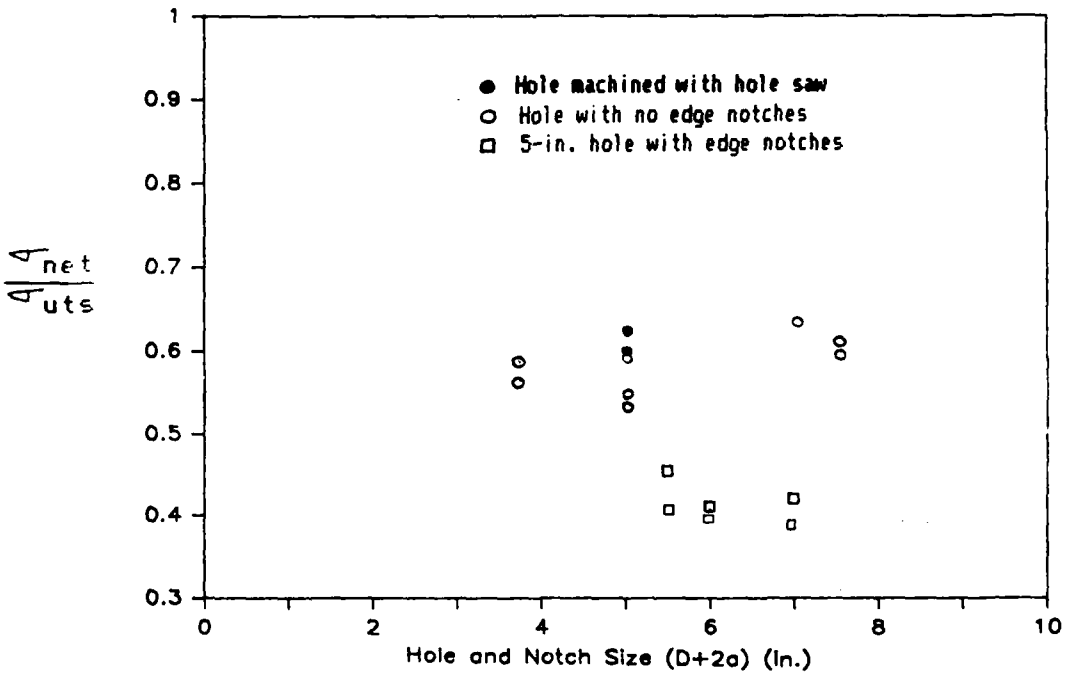

FIGURE 16

Failed Panel with a 5.0 inch Hole

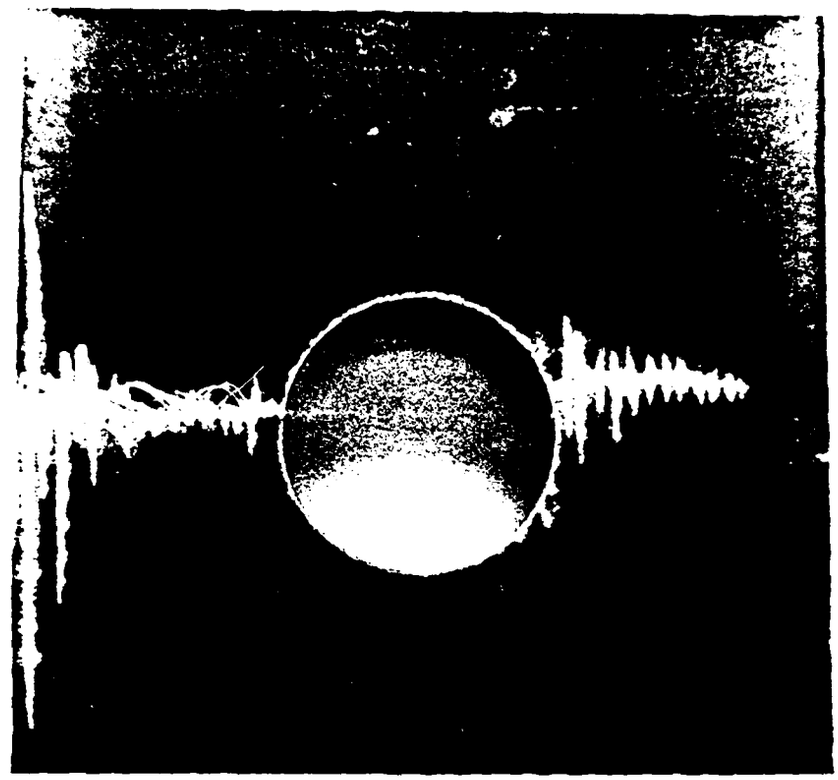

FIGURE 17

Validity of Stress Concentration Model as a Function of Hole Diameter using Measured Ultimate Tensile Strength

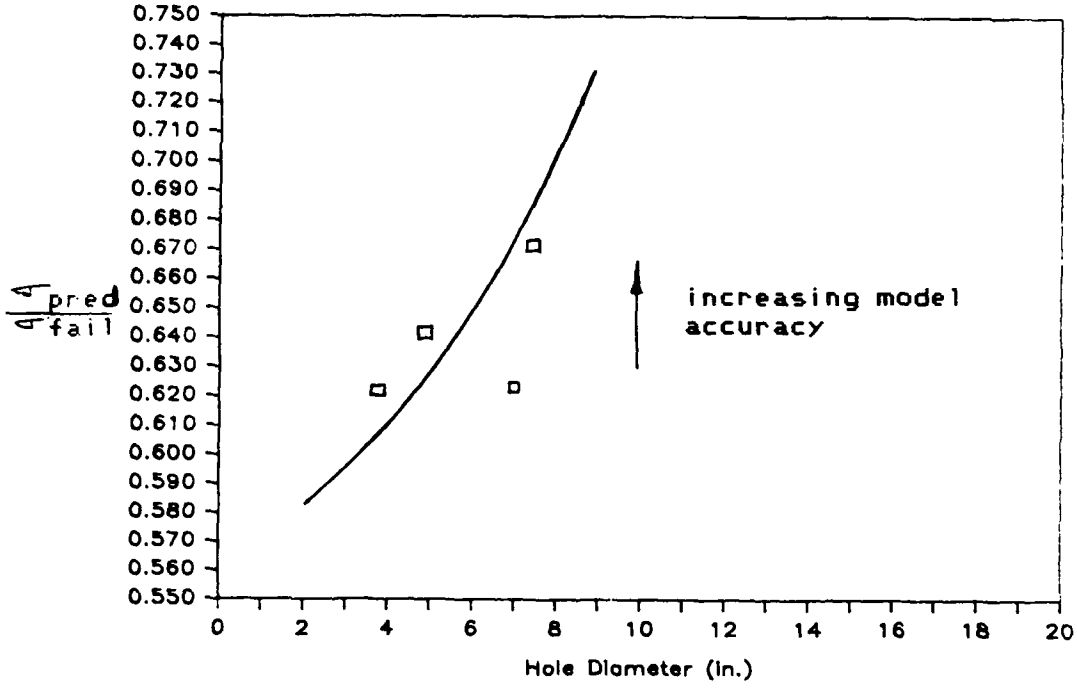

FIGURE 18

Failure Stress as a Function of Hole Diameter Compared with Predictions from Stress Concentration Model

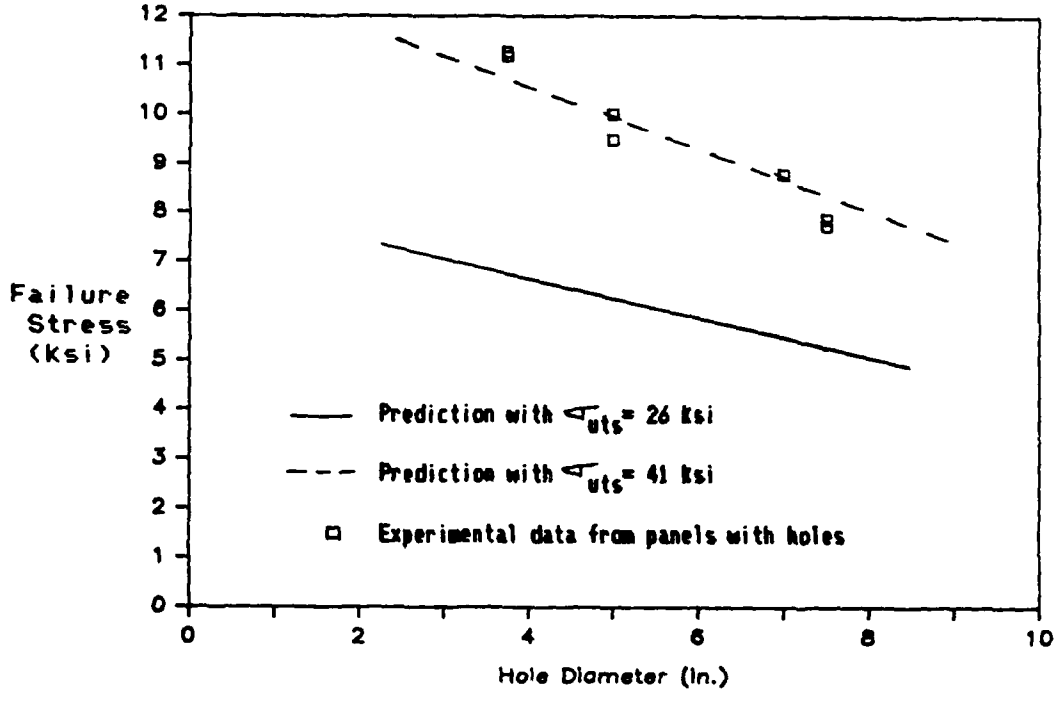

FIGURE 19

Crack Propagation in a
Double-Cantilever Beam Specimen

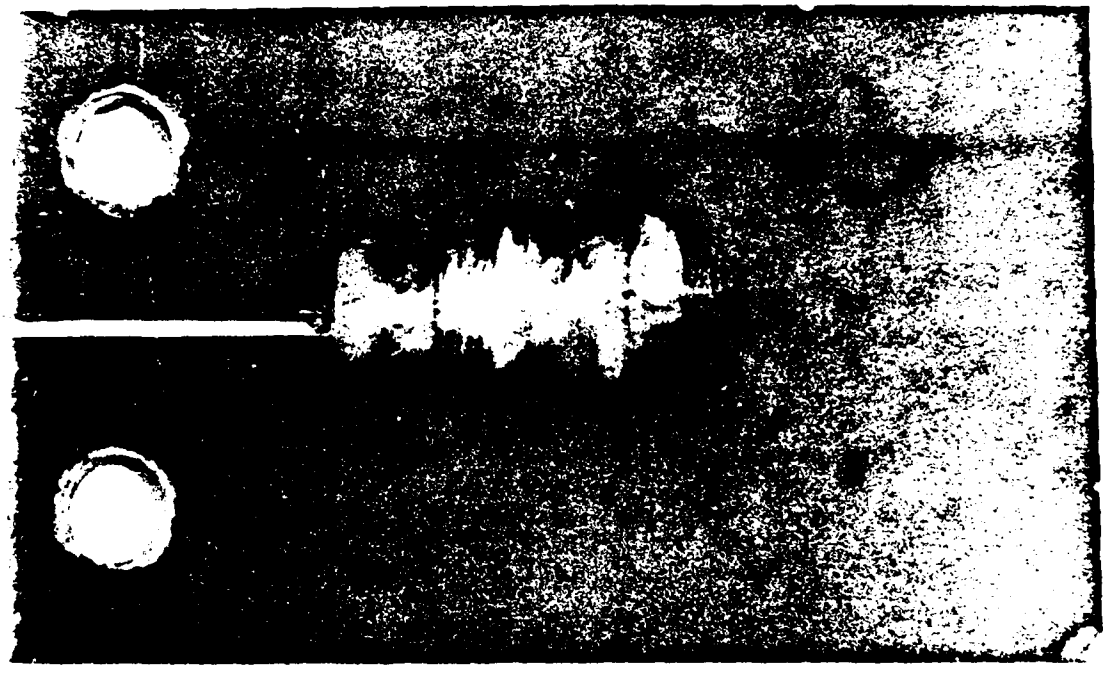

FIGURE 20

K_Q versus Crack Length Using Orthotropic
K-Calibration from Reference 18 (Longitudinal Direction)

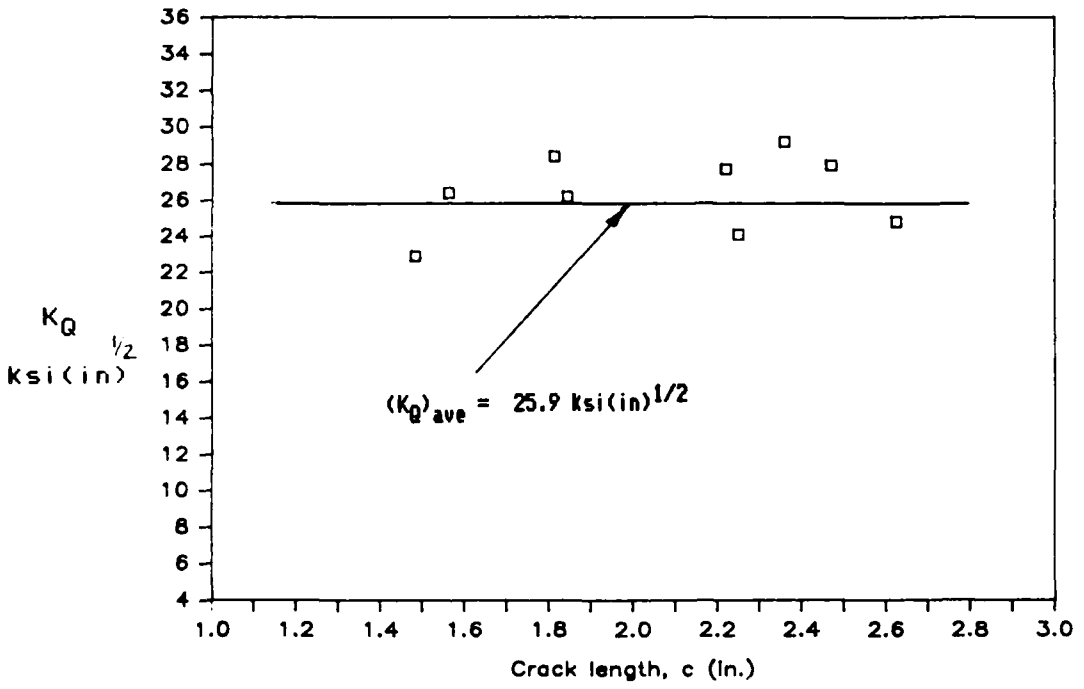

FIGURE 21

Predicted Failure Stress Based on Fracture Mechanics Versus Experimental Data as a Function of Notch Length at the Edge of a 5.0 inch Hole

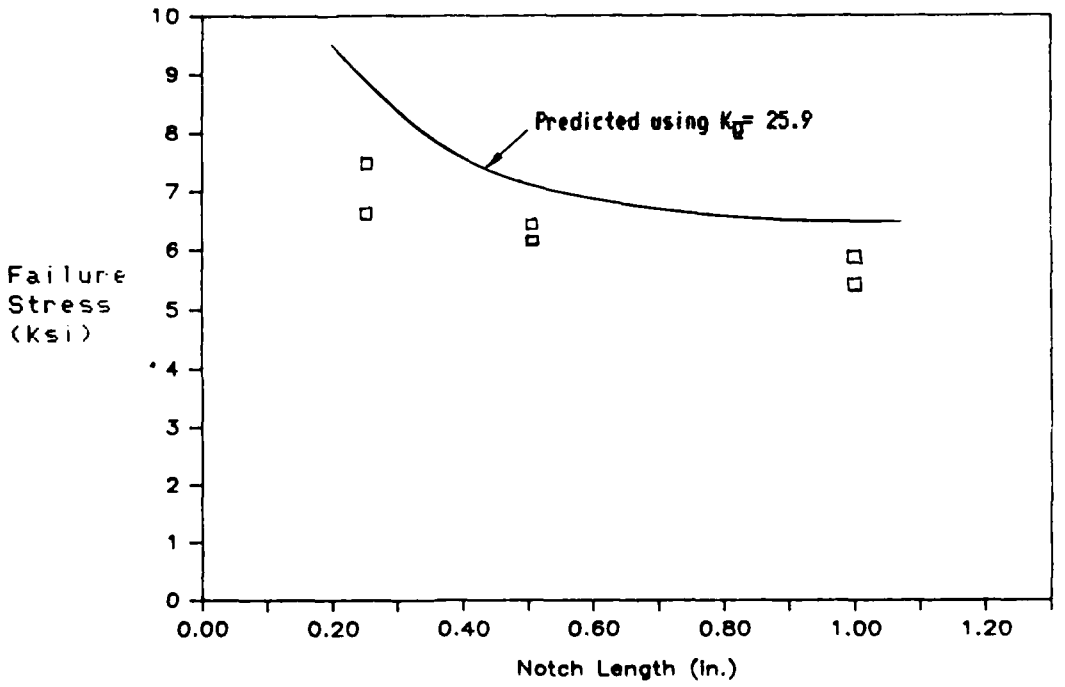

FIGURE 22

Fatigue S-N Curve in Saltwater
Environment for GRP Material in Reference 26

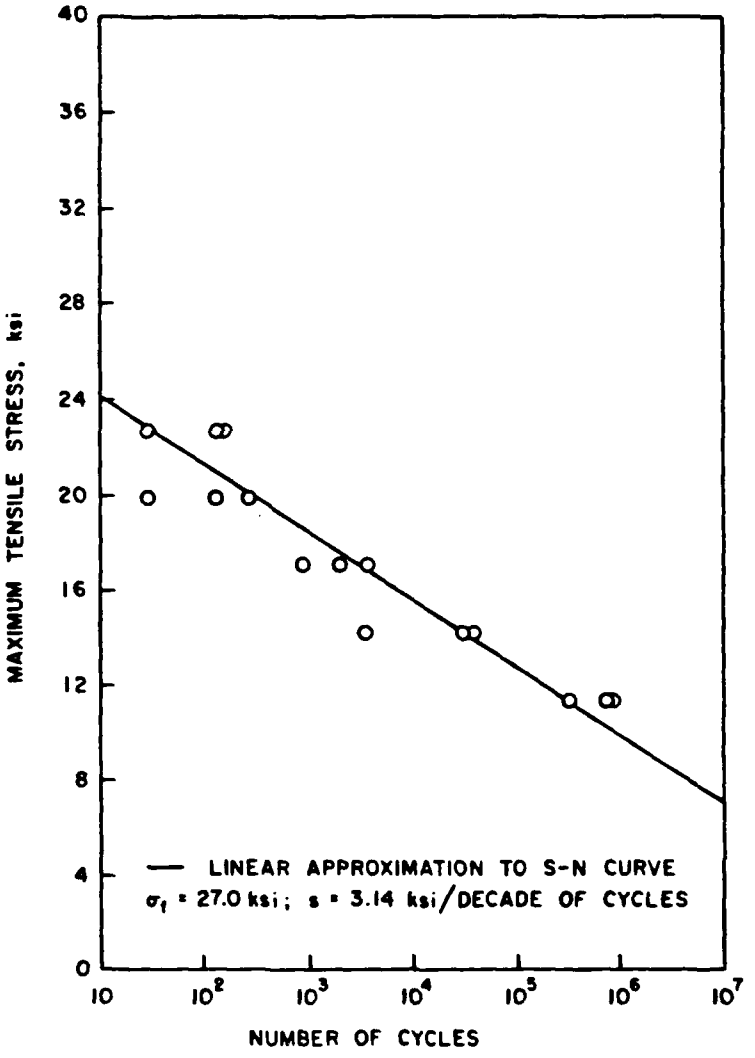

FIGURE 23

Predicted Fatigue S-N Curve for Material
in this Study in a Salt Water Environment
With no Cutout, Based on Trend in Figure 22

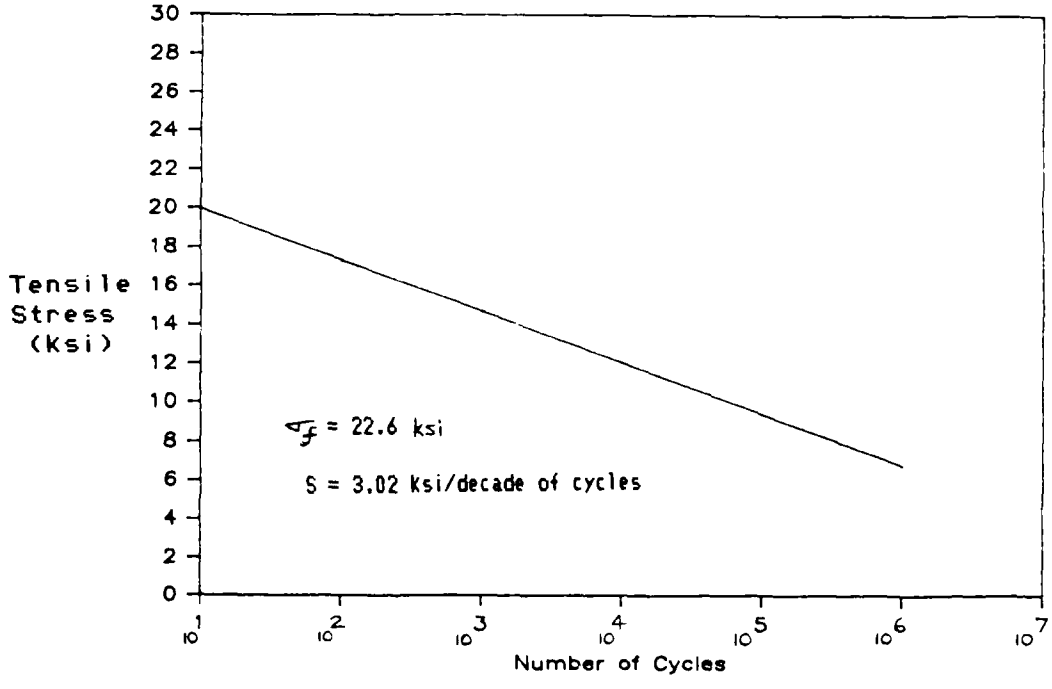

FIGURE 24

Predicted Fatigue Failure Stress in
Salt Water as a Function of
Hole Diameter and Number of Cycles

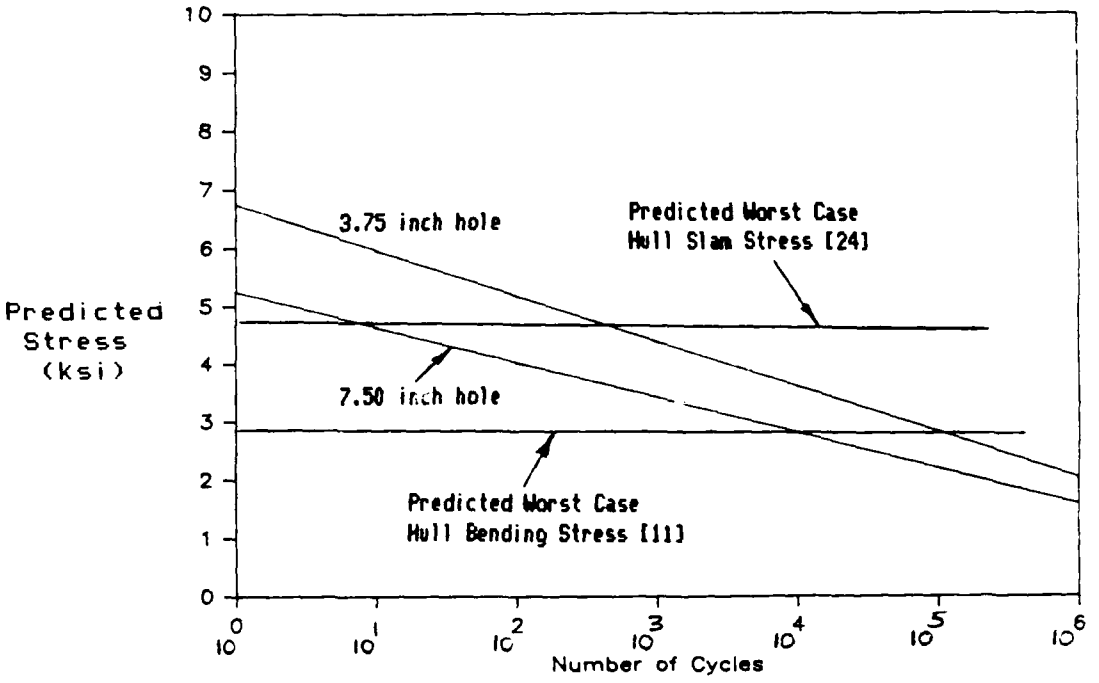

FIGURE 25

Cycles to Initial Crack Extension from an Edge Notch at a 5.0 inch Hole as a Function of Applied Stress and Notch Length (Based on Fatigue Crack Model [26])

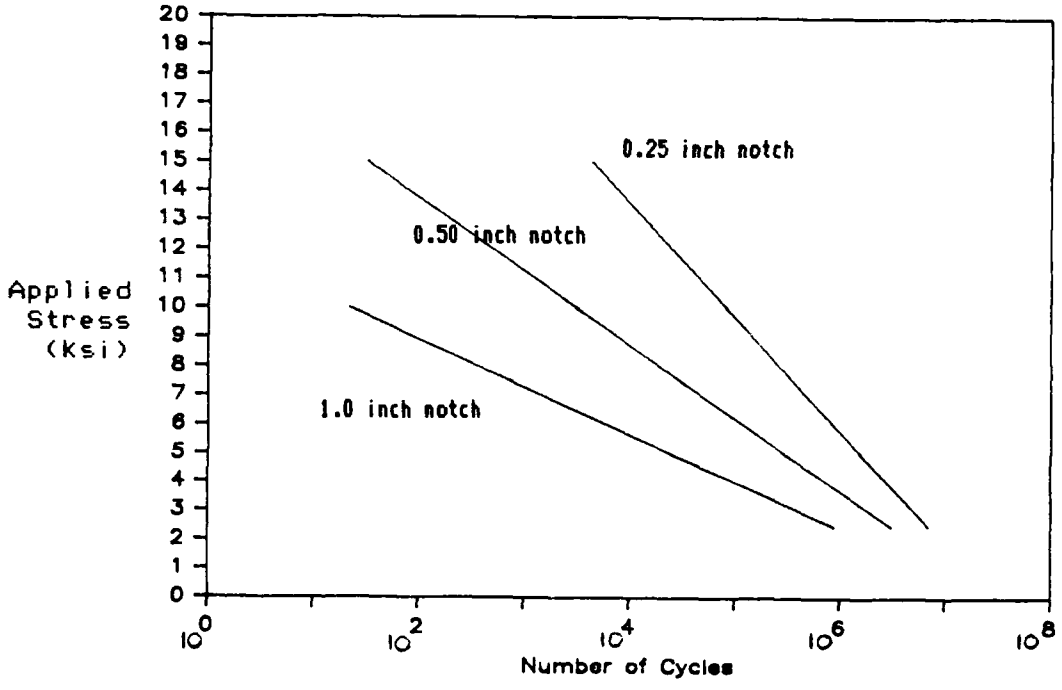

FIGURE 26

Crack Propagation Rate as a Function of Crack Length

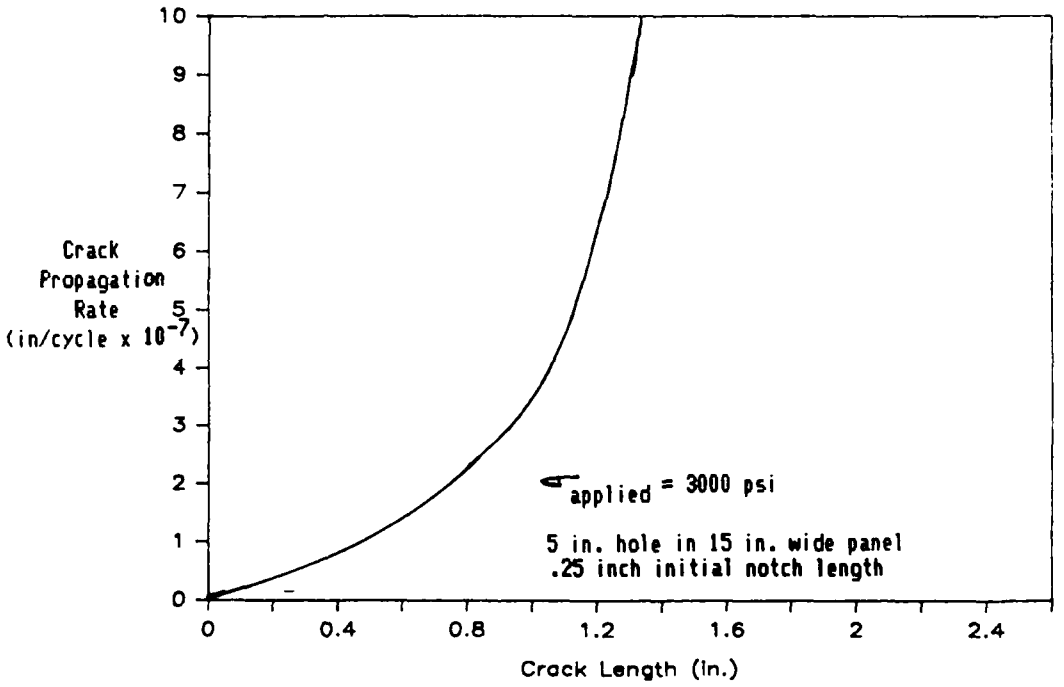

FIGURE 27

Factor of Safety Model

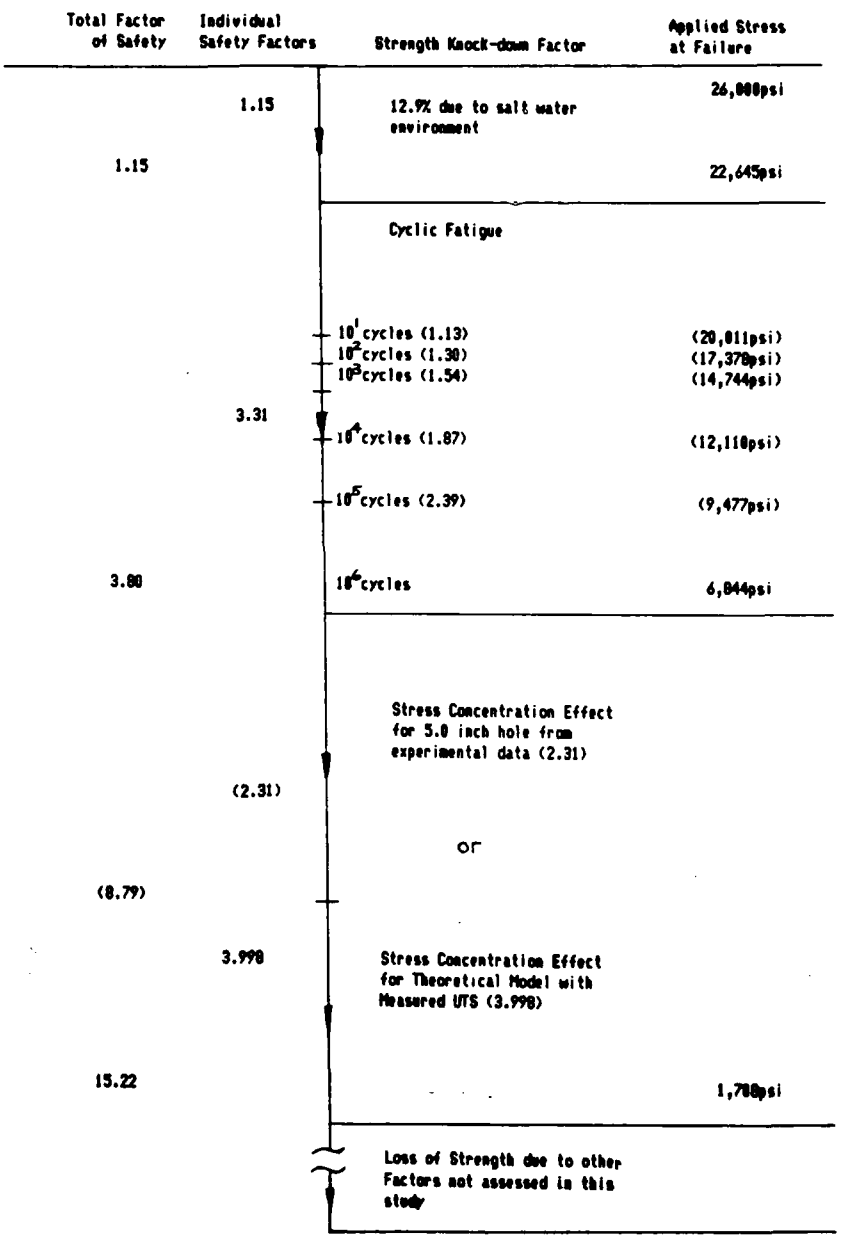

APPENDIX A

Notch Insensitivity Model Calculation

$$\sigma_{net} = \sigma_{uts} \frac{(W-2a-d)}{W}$$

where σ_{uts} = 26,000 psi
W = 15 inches
d = variable
2a = variable

Hole Diameter(d)	Crack Length(a)	Strength on the Remaining Net Cross-Section(σ_{net})
3.75in.	1.00in.	16,033psi
	0.50in.	17,767psi
	0.25in.	18,633psi
	0	19,500psi
5.00in.	1.00in.	13,867psi
	0.50in.	15,600psi
	0.25in.	16,467psi
	0	17,333psi
7.50in.	1.00in.	9,533psi
	0.50in.	11,267psi
	0.25in.	12,133psi
	0	13,000psi

APPENDIX B

Calculation of the Isotropic Stress Concentration Factor in a Finite Width Plate with a Circular Hole

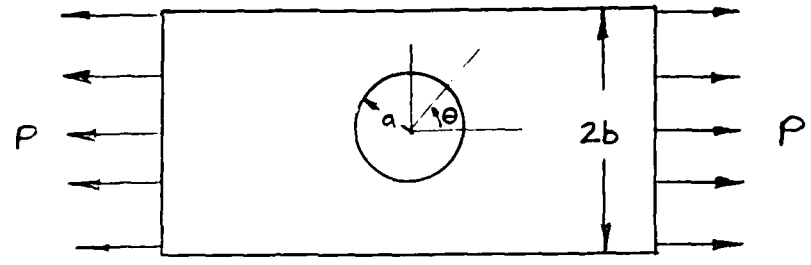

where λ = a/b

σ_θ = tensile force along the contour of the hole

P = uniform applied tensile force

From Savin [15] we get a Table of σ_θ/P for θ and λ

θ	λ=0	λ=0.1	λ=0.2	λ=0.3	λ=0.4	λ=0.5
0°	-1.00	-1.03	-1.11	-1.26	-1.44	-1.58
15°	-0.73	-0.74	-0.82	-0.95	-1.12	-1.32
30°	0	-0.01	-0.06	-0.15	-0.30	-0.51
45°	+1.00	+1.00	+1.00	+0.98	+0.91	+0.77
60°	+2.00	+2.01	+2.07	+2.15	+2.25	+2.32
75°	+2.73	+2.74	+2.85	+3.03	+3.32	+3.72
90°	+3.00	+3.03	+3.14	+3.36	+3.74	+4.32

In this Table Savin shows that the maximum stress is present at the hole edge. Therefore it is only necessary to consider the most limiting case of σ_θ/P at $\theta = 90^\circ$. The value for λ is calculated for the hole diameter (2a) and panel width (2b) for the particular specimen. Table interpolation then yields the proper value for σ_θ/P.

The stress that would be present at the edge in the absence of the hole or discontinuity is P and the stress with the hole or discontinuity is the value of σ_θ/P. The definition of the stress concentration factor will now allow K_T to be calculated.

Once the stress concentration factor for the geometry under consideration is known the predicted failure stress for the material can be related by:

$$\sigma_{fail} = \sigma_{uts}/ K_T$$

For the specimen width (15in.) and hole diameters observed the isotropic stress concentration factors and predicted failure stresses, based on an ultimate tensile stress of 26,000 psi, are

Hole Radius	Specimen Half Width	λ	K_T	σ_{fail}
1.875in.	7.500in.	0.500	3.250	8,000psi
2.500in.	7.500in.	0.333	3.486	7,457psi
3.500in.	7.500in.	0.467	4.126	6,300psi
3.750in.	7.500in.	0.500	4.320	6,018psi

APPENDIX C

Correcting the Isotropic Stress Concentration Factor to Account for Anisotropicity

$$K_{Torthotropic} = 1 + \sqrt{2\left(\sqrt{\frac{E_Y}{E_x}} - \nu_{xy} + \frac{E_Y}{2G_{xy}}\right)}$$

$$K_{Tisotropic} = 3$$

$$f = \frac{K_{Torthotropic}}{K_{Tisotropic}}$$

For the material reported in Table 4

$$K_{Torthotropic} = 1 + \sqrt{2\left(\sqrt{\frac{1.9}{1.7}} - 0.19 + \frac{1.9}{2(.45)}\right)}$$

$$K_{Torthotropic} = 1 + (5.95659)^{1/2}$$

$$K_{Torthotropic} = 3.44$$

This value is now used with the isotropic stress concentration factor such that

$$f = 3.44/3.00$$

$$f = 1.1468$$

This correction factor can now be applied to the values for the isotropic stress concentration factor in Appendix B. The corrected orthotropic values are presented in Table 5.

APPENDIX D

K_I Calculation using the LEFM Model for Notched GRP Panels which were Tested in Tension to Failure

In this calculation the Stress Intensity Factor K_I at failure in each of the notched panels is calculated. The basis for the calculation is the use of a compendium of stress intensity factors for the geometry under consideration. Figure 5 is a graph from such a compendium [17] and is used to calculate K_I in the panels in this study.

The first step is to calculate the value of K_o for the failed panel using

$$K_o = \sigma_f \sqrt{\pi a}$$

where

σ_f = failure stress

a = crack length

This value for K_o is then corrected for the geometry by using the relation (K_I/K_o). In the graph in Figure 5 this relation is a function of the hole radius (R) to the panel width (b) and the crack length (a) to the panel width (b). For the specimen geometries listed this becomes

Specimen	R/b	a	a/b	K_{I/K_o}
6	0.33	3.5	.466	1.20
7	0.33	3.5	.466	1.20
8	0.33	3.0	.400	1.10
9	0.33	3.0	.400	1.10
10	0.33	2.75	.367	1.00
11	0.33	2.75	.367	1.00

The stress intensity factor may now be calculated from the experimental results using

Specimen	σ_f	K_o	K_I(ksi(in)$^{1/2}$)
6	5835	19,347	23.2
7	5350	17,742	21.2
8	6396	19,635	21.6
9	6255	19,202	21.1
10	7473	21,965	21.9
11	6609	19,426	19.4


DATE
FILMED
28